Title:

- Structural basis of CO_2 valence coding in *Drosophila*

Authors:

Example: Javorski Dominik[1], Bergkirchner Beate[1], Ensinger Gernot[1], Lingl Alexander[1], Navolic Jelena[2], Batawi Ashwaq[3], Hummel Thomas[1]

Affiliations:

[1]Department of Neurosciences and Development, University of Vienna, Djerassiplatz 1, 1030 Vienna, Austria

[2]Center for Molecular Neurobiology Hamburg, University Medical Center Hamburg-Eppendorf, Falkenried 94, 20251 Hamburg, Germany

[3]King Abdulaziz University, 21589 Jeddah, Saudi Arabia

*Corresponding author: Email: thomas.hummel@univie.ac.at

Abstract

In the olfactory system, glomerular sensory channels of single receptor identity support reliable odor recognition for appropriate approach or avoidance behaviors. For many olfactory stimuli, the assigned sensory value is innate but modulated by the internal state and previous experiences. How context-dependent modulation of innate valence coding supports distinct behavioral responses is poorly understood. Here we show that CO_2 sensory information in *Drosophila*, intrinsically aversive but modified by attractive food signals, diverges from the canonical glomerular channel already in the antennal lobe and is relayed via the polarized local interneuron LN23. LN23 relays sensory input via an extraglomerular CO_2 pathway and manipulation of LN23 activity revealed a dominant role in CO_2-induced avoidance behavior. The extraglomerular CO_2 pathway projects to the posterior lateral protocerebrum (PLP) adjacent to the canonical Lateral Horn (LH) olfactory processing center and segregates into anatomically distinct valence channels. Connectome data together with functional characterization showed the convergence of parallel CO_2 channels onto two interconnected third-order neurons. These neurons integrate additional sensory modalities via distinct mechanisms: while the glomerular CO_2 pathway converges with food relay neurons onto separated dendritic domains of the PD5 interneuron in the LH, the extraglomerular pathways integrating CO_2 information with antennal humidity and temperature modalities establish antagonistic inputs onto the PLP interneuron PV9. This early anatomical divergence of a

defined olfactory channel followed by separated multi-modal integration provides a structural basis for context-dependent valence coding and appropriate behavioral responses.

56 **Introduction**

57 The ability to recognize and react to environmental stimuli is essential for the survival of
58 animals. Insect olfactory systems allow the sensing and integration of volatile signals to
59 identify food resources and avoid potential threats (Wilson, 2013). Although CO_2 is a
60 component of the atmosphere, local changes in ambient CO_2 levels can induce context-
61 dependent behavioral responses (Faucher et al. 2006; Hansson & Stensmyr, 2011). Walking
62 *Drosophila* show robust CO_2-induced avoidance (Suh et al. 2004; Kwon et al. 2007; Faucher et
63 al. 2006), while in more aroused states such as flight or foraging, CO_2 becomes an attractive
64 olfactory cue (van Breugel et al. 2018) which is linked to dopamine levels affecting mushroom
65 body output neurons (Lewis et al. 2015; Sachse & Beshel 2016). At the circuit level, prolonged
66 CO_2 exposure leads to olfactory habituation, mediated by plasticity of GABAergic interneurons
67 in the antennal lobe (Das et al. 2011; Olsen & Wilson, 2008; Nagel & Wilson, 2016; Sachse et
68 al. 2007; Semelidou et al. 2018). Interestingly, *Drosophila* avoidance behavior directly
69 correlates with the activity of CO_2-specific olfactory receptor neurons (MacWilliam et al.
70 2018), raising the question of how CO_2-induced sensory activity is transformed into central
71 valence representations and modulated to support context-dependent behavior (Frechter et
72 al. 2019).

73 The peripheral CO_2 circuit follows the canonical organization of olfactory sensory channels. A
74 single population of ORNs (ab1C) co-express the gustatory receptors Gr21a and Gr63a and
75 projects ipsilaterally to the V glomerulus in the ventral antennal lobe (Suh et al. 2004; Kwon
76 et al. 2007; Vosshall & Stocker 2007). CO_2 sensation is transmitted to higher brain centers
77 through two glomerular PNv types: a bilateral cholinergic PN (PNv^{bi}) projecting to both the
78 mushroom Body (MB) and lateral Horn (LH), and a LH specific relay via a unilateral PN (PNv^{uni})
79 (Grabe et al. 2016; Lin et al. 2013; Sachse et al. 2007; Tanaka et al. 2012). Although distinct
80 spatial LH domains encoding opposite hedonic values and odor intensity have been identified
81 (Frechter et al. 2019; Das Chakraborty et al. 2022), glomerular PNs provide synaptic input to a
82 diverse set of LH neurons making the identification of central brain representation and
83 context-dependent modulation of a given sensory channel difficult (Dolan et al. 2019; Scheffer
84 et al. 2020).

85 Here we describe the identification of a novel CO_2 relay channel, morphologically and
86 functionally separate from the canonical glomerular circuit via a polarized olfactory
87 interneuron, LN23. The LN23 pathway mediates a robust CO_2-induced aversion largely
88 unaffected by glomerular circuit plasticity but allows early multi-modal integration.
89 Furthermore, the parallel pathways of glomerular and extraglomerular PNs converge onto a
90 small group of LH interneurons as the core domain for CO_2 valence coding in the central brain.

91 **Material and Methods**
92

93 ***Drosophila* Stocks**
94

95 VT031497 (PNv^{bi} Gal4 and the alternative line: R53A05; BDSC#38859; BDSC: Bloomington
96 *Drosophila* Stock Center), NP7273 (PNv^{uni} Gal4), R44A02 (LN23 Gal4; BDSC#50196) were used
97 to target neurons PNv^{bi}, PNv^{uni} and LN23 respectively. LN23-lexA (BDSC#53644) and PNv^{bi}-lexA
98 (VT031497 lexA) were used in sybGRASP (BDSC#93197 / reverse direction BDSC#64315) and
99 tGRASP (BDSC#79040/reverse direction BDSC#79039) experiments to express the
100 postsynaptic GFP fragment. Gr21-Gal4 (BDSC#57600) was used to target ORNs that project
101 specifically to the V-glomerulus. To target LNv1 and LNv2, we used NP1227P from the Max
102 Planck Institute and NP2426-P from the Kyoto Stock Center. The Gal4 driver line BDSC #40444
103 was used for l2LN19. UAS-*shibire*^{ts} (Gift from Barry Dickson) was used to inhibit neurons at
104 restrictive 31°C. UAS-ReaCh (BDSC#53741) was used in optogenetic experiments to artificially
105 activate specific neuronal subsets which are labelled by the Gal4 lines. CantonS and w1118
106 wild-type flies were used for control experiments. The $Gr63a^1$ (BDSC#9941) mutant stock was
107 used in behavior experiments as a control for flies which are unable to detect CO_2. In addition
108 to our main LN23 line (BDSC#50196) an additional line also labeling LN23 (BDSC#48408) was
109 used for optogenetics. UAS-CaLexA (BDSC#66542) was used in combination with the Gal4 lines
110 to label active neurons. To further activate or silence specifically active neurons, a CaLexA
111 stock without GFP was used (BDSC#66543) in combination with lexAop-ReaCh or lexAop-shi^{ts}
112 respectively. UAS-*DenMark::cherry* was used to label dendrites of neurons while UAS-*syb::GFP*
113 and UAS-*syt::GFP* specifically labeled presynaptic terminals. To confirm the location of active
114 T-bars in LN23 and PNv^{bi} neurons, we also applied UAS-*brp::GFP* (BDSC#36291 and
115 BDSC#36292).

116 **Immunohistochemistry**
117

118 Flies were dissected in PBS (phosphate buffer solution) and brains were fixed in 2% PFA
119 (Paraformaldehyde). After the fixation brains were washed 3 times with 0.3% PBT (phosphate
120 buffer with TritonX) and then blocked with goat serum. After 1 hour of blocking the first AB
121 (Antibody) was applied and the brains were kept in a 4°C fridge overnight. The next day brains
122 were washed again 3 times before applying the second AB. After the staining protocol was
123 complete, brains were mounted and subsequently scanned with a confocal microscope. Anti-
124 Ncad rat (1:10, DHSB) was used to label all neuropiles in the fly brain in all experiments. For
125 CaLexA experiments anti GFP rabbit (1:5000, Invitrogen) was used additionally to enhance the
126 signal strength, according to Masuyama et al. (2012). GRASP experiments, DenMark and
127 labeling of presynaptic terminals (*syt::GFP* and *syb::GFP*) didn't require any antibodies besides
128 anti-Ncad since the endogenous signal was sufficient and changes after CO_2 incubation should
129 not be distorted. For MCFO, first Antibodies were Anti-Ncad rat (1:10) or Anti-ollas rat
130 (1:2000), Anti-flag mouse (1:2000) and Anti-HA rabbit (1:2000). As second antibodies anti-rat
131 647 (1:500), anti-mouse (highly cross-absorbed, 1:300) and anti-rabbit (1:500) were applied.

132 **MCFO (Multicolor flip-out)**
133

134 To label single cells in a usually rather broad expressing Gal4-line, we took advantage of a
135 method established by Nern et al. 2015, called MCFO. They recombined four constructs,
136 consisting of an UAS-site, followed by a stop-cassette to suppress transcription and one of
137 four different transmembrane proteins, which can, if expressed, be labeled via antibodies.
138 These four independent constructs can also be expressed together in the same cell, which
139 leads to a mixture of colors and increased probability of one cell getting labeled in one distinct
140 color. The stochastic excision of the stop cassette is achieved by a heat sensitive enzyme,
141 whose activation is triggered by incubating the flies at 37°C in a water bath.

142 **GRASP**
143

144 To visualize synaptic contacts two different GRASP tools were used. SybGRASP is activity
145 dependent because one fragment of GFP is located on vesicle membranes. As vesicles fuse
146 with the presynaptic membrane, which is dependent on incoming action potentials, the large
147 GFP fragment is exposed in the synaptic cleft and can reconstitute with the small GFP fragment

148 located on the postsynaptic membrane (Macpherson et al. 2015). tGRASP, or targeted GRASP
149 (Shearin et al. 2018), is activity independent and the two GFP fragments are bound to pre and
150 postsynaptic specific proteins (Cacophony and Telencephalin respectively). A comparison of
151 these two GRASP techniques allowed us to make assumptions about changes of synaptic
152 activity and changes to synaptic density. No antibodies against GFP were used since the
153 endogenous expression was sufficient. GFP intensities were quantified with FIJI, which is
154 measured as the mean gray value of a defined region of interest (ROI) above a threshold. To
155 subtract the mean gray value of the background noise, intensity was measured in another
156 glomerulus (same size of ROI) which was not showing any signal. Each datapoint in the
157 diagrams represents one quantified glomerulus. The same applies to intensity measurements
158 for the following two sections.

159 **DenMark::cherry / Syt:GFP, syb::GFP**
160

161 UAS-*syt::GFP* and UAS-*syb::GFP* were used to label presynaptic terminals of target neurons.
162 Synaptotagmin (*syt*) and synaptobrevin (*syb*) are proteins of the vesicle membrane and
163 therefore a Gal4 driven expression of the GFP tagged proteins shows strong signal in the
164 presynaptic terminals. UAS-*DenMark* (Dendritic Marker) is a somatodendritic marker (*cherry*)
165 to label dendrites. *GFP/Cherry* intensities were quantified with FIJI.

166 **CaLexA**
167

168 CaLexA (Masuyama et al. 2012) was used to label active cells. It is based on the NFAT
169 transcription factor, which is calcium responsive. As Ca^+ enters a cell, a chimeric lexA-VP16-
170 NFAT, enters the nucleus where expressed lexA can bind to lexAop inducing the expression of
171 GFP. The stronger and longer the excitation lasts, higher GFP intensities are expected. GFP
172 levels were quantified in FIJI as it was described in the section about GRASP. There was no
173 selection for gender and all flies tested were 2 days old at the start of the experiments. In the
174 experimental condition where flies were kept under the elevated level of 5% CO_2 the duration
175 of the exposure was 3 days. We also used a CaLexA construct where expressed lexA is not
176 expressing GFP but instead driving the expression of a temperature sensitive shibire protein
177 to silence neurons. Further we also used this stock in combination with lexA driven expression
178 of ReaCh to specifically further activate physiologically active neurons. 99% spermidine was
179 used as an inhibitor to GR21a receptors. 5µl were put on a small piece of cotton which was

180 then transferred to a vial containing the flies which were used in the experiments after 3 days
181 of exposure.

182 **Behavioral experiments**
183

184 For behavioral experiments, flies were kept in total darkness, in 25°C incubators in vials
185 containing fly food. Flies which were used in optogenetics were raised on fly food containing
186 all-trans-retinal to enhance their response to light exposure (Vilinsky et al. 2018). All flies were
187 age matched and tested when they were 3-4 days old. Since there was no observed difference
188 between male and female flies, both sexes were used in all behavioral experiments. As we did
189 not observe any behavioral artifacts caused by either green or red LED light we opted for the
190 green LEDs, since they elicited a stronger response in the flies (compared to Inagaki et al.
191 2014).

192 Flies were immediately transferred to empty vials which can be connected to the CO_2 or
193 optogenetic setup after they were taken out of the incubators. The whole procedure was also
194 done in darkness (red light was used to be able to handle the flies, which is barely visible for
195 the flies) to minimize visual distraction affecting the fly's behavior. The whole apparatus was
196 shifted sideways, and the flies were gently moved to the elevator segment of the setup. The
197 elevator was lowered to a position short above the decision point and the flies were given 60
198 seconds rest. After the resting period either a green LED light or CO_2 flow was activated and
199 the elevator was lowered to the decision point.

200 The animals were given 20 seconds to move inside the behavioral setup and make a choice.
201 Afterwards the elevator was pulled up again, so that the flies remained in either the test tube,
202 control tube or the central elevator area. Each of these populations was counted and a
203 preference index (PI) calculated, defined as the percentage of flies located in the control arm
204 (air-filled /dark) of the setup, minus the percentage of flies located in the test arm (CO_2
205 filled/light). Since in some of the tested populations, a few animals remained in the central
206 elevator part of the arena, their decision was defined as neutral. Their number was divided by
207 two and added to both the test and control population for the PI. Each datapoint in the
208 diagrams represents the PI of a group of flies (n=15-40).

209

210 **Hemibrain analyses**
211

212 Connectivity data were obtained from the neuPrint interface (neuPrint, Janelia Research
213 Campus; https://neuprint.janelia.org/) built on the Hemibrain connectome (Scheffer et al.
214 2020). It was used to study and model the neurons involved in the V-circuit. The main goal
215 was to identify synaptic connectivity between the different layers of information processing
216 within the circuit. Finally, the putative circuit was reconstructed in 3D and PN/LN output zones
217 were identified. Neuronbridge.janelia.org was used to gather 3D images from l2_PNm17 and
218 sm_PNm1. FlyWire.ai was a tool to quickly get information about the predicted
219 neurotransmitter identities of neurons.

220 **Statistics**
221

222 All diagrams and statistical analyses were done by using GraphPad Prism 9 software. Normally
223 distributed data were compared with a student's t-test, whereas datasets that did not meet
224 normality assumptions were analyzed with a Mann–Whitney U test. Behavioral data spanning
225 multiple days were tested with a one-way ANOVA. Statistical significance is indicated in the
226 figures by asterisks, with $p < 0.05$ (*), $p < 0.01$ (**), $p < 0.001$ (***), and $p < 0.0001$ (****).

227

228 **Results**
229

230 **Glomerular circuit dynamics of CO_2 perception**
231

232 The V glomerulus at the ventral AL surface is innervated by a single population of about 40
233 CO_2-sensitive olfactory receptor neurons (ORNv) expressing the two gustatory receptors
234 GR21a and GR63a (Kwon et al. 2007; Jones et al. 2007) (Fig.1A-B). Each ORNv axon forms 3-5
235 terminal branches tightly packed in a non-overlapping fashion with other ORN terminals (Fig.
236 1, C-C´´), providing sensory input to glomerular inter- and projection neurons (Fig1D-G´)
237 (Grabe et al. 2016).

238 To identify relay neurons of the V glomerulus with different physiological properties we
239 screened a collection of Gal4 lines using the CaLexA activity reporter to compare intracellular

240 Ca^{2+} levels under ambient CO_2 conditions (Koyama et al. 2021; Masuyama et al. 2012) (Fig. 1H-
241 O). Gal4 lines for ORNv show strong CaLexA reporter activity (Fig.1H), in line with a high default
242 activity of CO_2-receptive sensory neurons due to the absence of $GABA_B$-mediated presynaptic
243 inhibition (MacWilliam et al. 2018; Olsen & Wilson, 2008; Root et al. 2008). In contrast to
244 elevated Ca^{2+} levels in ORNv, the two uniglomerular PN classes of the V glomerulus, unilateral
245 V_l2PNs (PNv^{uni}) and bilateral V_ilPNs (PNv^{bi}, Fig. 1D) do not show any significant level of
246 CaLexA activation under ambient air conditions (Fig. 1I, J). Two main classes of local
247 interneurons, LNv1 and LNv2 display moderate levels of CaLexA activity at atmospheric CO_2
248 levels (Fig. 1K, L). A strong CaLexA-GFP signal, comparable to ORNv can be observed for l2LN23
249 (LN23), a less characterized olfactory class of sparsely innervating local interneurons (Fig.1F,
250 F', M and N) (Liou et al. 2018). Fluorescence signal of Ca^{2+}-induced GFP expression quickly
251 decreases in LN23 following sensory deprivation in adult flies via removal of both antennae
252 (Fig.1O). Furthermore, an extended exposure to the ORNv inhibitor spermidine (MacWilliam
253 et al. 2018) results in a reduced CaLexA activity not only in ORNv, but also LN23, indicating a
254 preferred physiological coupling of sensory neurons to LN23 interneurons under ambient CO_2
255 conditions (Fig. 1O).

256 A predominant relay of CO_2-induced sensory activity by LN23 is supported by the modified
257 activity-dependent GRASP technique (Macpherson et al. 2015). Expression of the presynaptic
258 *syb::GFP*$^{1-10}$ in ORNv and the postsynaptic *GFP*^{11} in AL neurons revealed a significantly stronger
259 GRASP signal for ORNv→LN23 connectivity compared to the ORNv→PNv^{bi} synaptic activity
260 (Fig.2F and G). Similarly, the activity-independent tGRASP (Shearin et al. 2018) is most
261 prominent for ORNv→LN23 (Fig.2I and J), which is in line with connectome data
262 (neuPrintExplorer, hemibrain; Scheffer et al. 2020; Schlegel et al. 2021). In summary, ORNv
263 activity at ambient CO_2 levels seems to be mainly represented by the LN23 class of local
264 interneurons and less by glomerular PN relay neurons, thereby identifying a new circuit
265 component for the ORNv-induced behavioral aversion.

266

267

268

269

270 **Cell type plasticity of glomerular relay neurons following chronic CO_2 stimulation**
271

272 We next determined how the overall activity of V glomerulus relay- and interneurons changes
273 following long-lasting sensory stimulation. Adult *Drosophila melanogaster* avoids ambient
274 levels of CO_2 in the T-maze choice assay (Faucher et al. 2006; Suh et al. 2004) (Fig. 2A) but
275 shows behavioral habituation following chronic CO_2 exposure (Das et al. 2011, Fig. 2B, C). The
276 reduction of CO_2-induced aversive responses is associated with an increase in the synaptic
277 volume of the V glomerulus (Fig.2D; Sachse et al. 2007 and Das et al. 2011). At the ORN level,
278 mosaic analysis revealed an extension in the surface area and size of individual synaptic
279 boutons of ORNv axons (Fig.2E). Compared to ambient CO_2 levels, prolonged elevated CO_2
280 (5%) sensation results in neuron-type specific changes of CaLexA activity (Fig. 1 H'-N')
281 (Masuyama et al. 2012). While PNv^{bi} neurons showed a strong increase in Ca^{2+} levels following
282 CO_2 habituation (Fig.1I´), whereas no CaLexA-dependent GFP expression was observed in
283 PNv^{uni} (Fig.1J´), indicating different physiological properties of the two main glomerular CO_2
284 relay channels (Lin et al. 2013). In addition to chronic CO_2 stimulation, short pulses of elevated
285 CO_2 also did not induce Ca^{2+}-mediated-GFP expression in PNv^{uni} (Fig.1O). No significant
286 changes in CaLexA-GFP levels could be detected for LN23 neurons following prolonged CO_2
287 exposure compared to the already high expression at ambient CO_2 conditions (Fig1M´, N´, O).

288 As GABAergic local interneurons are associated with olfactory habituation (Das et al. 2011;
289 Sadanandappa et al. 2013) we compared changes in CaLexA activation in LNv1 and LNv2 (Das
290 et al. 2011, Sachse et al. 2007). While an increase in the Ca^{2+} reporter signal could be observed
291 for both LN types following chronic CO_2 exposure, the activity of LNv1 is significantly higher
292 compared to LNv2 (Fig.1K' and L´). In line with the cell-type specific CaLexA expression,
293 previous connectome analysis showed significant differences of LN input for CO_2 relay
294 neurons: (neuPrintExplorer, hemibrain): While both PNv^{uni} and LN23 do not receive major LN-
295 type input, PNv^{bi} gains GABAergic modulation by lLN1 neurons ("bc" subtype, 16% of input)
296 and a group of multiple lLN2 neuron types (X, F, P, 19%) (Schlegel et al. 2021; Bates et al.
297 2020). These results indicate cell type specific physiological changes of glomerular neurons
298 following CO_2-induced behavioral habituation, in which PNv^{bi} shows dynamic changes in
299 glomerular connectivity while both PNv^{uni} and LN23 neurons maintained their characteristic
300 activity seen in ambient CO_2 conditions.

301 We next tested how the cell-type specific changes in neuronal activity during habituation
302 impact their synaptic connectivity within the V glomerulus. A strong increase of activity-
303 dependent sybGRASP levels for ORNv input onto PNv^{bi} could be detected following chronic
304 CO_2 stimulation (Fig.2F'). In contrast, no significant changes in sybGRASP levels were observed
305 for ORNv input onto LN23 (Fig.2G´). Of note, compared to ambient CO_2 conditions, the
306 standard deviation for ORNv→LN23 sybGRASP levels was reduced in flies chronically exposed
307 to CO_2, indicating that sensory input onto LN23 also increases in the context of habituation
308 (Fig.2H). In addition, activity-independent tGRASP expression showed that ORNs increase
309 their synaptic connections to the two main relay neurons, PNv^{bi} and LN23 (Fig.2I', J'), which is
310 in line with morphological changes of ORN axon terminals described above (Fig.2D, E).
311 Following prolonged CO_2 exposure, the PNv^{bi} class displayed increased sybGRASP levels on
312 PNv^{uni} and LN23 (Fig.2L-M'''), while no significant changes could be observed for LN23 on PNv^{bi}
313 (Fig.2N-N'''). Taken together, CO_2-induced ORNv activity seems to be relayed via two distinct
314 glomerular output channels dependent on the stimulus strength: LN23 neurons indicate
315 default ambient CO_2 levels while PNv^{bi} signals at conditions of extended elevated CO_2.

316

317 **Identity, innervation patterns and polarity of second-order CO_2 sensitive neurons**
318

319 To test if the difference in CaLexA activity might be related to the organization of presynaptic
320 sites within CO_2 relay neurons we visualized the active zones using *syt::GFP/brp::GFP*
321 transgenes together with the dendrite marker *DenMark::mCherry* (Kittel et al. 2006, Nicolai et
322 al. 2010; Wagh et al. 2006). PNv^{bi}, PNv^{uni} and LN23 differ significantly in their expression and
323 localization of presynaptic proteins within the dendritic compartment (Fig.3A-C). While PNv^{bi}
324 shows prominent dendritic *syt::GFP* localization throughout the glomerulus (Fig.3C), no
325 *syt::GFP* signal can be detected within PNv^{uni} dendrites (Fig.3A), indicating different cellular
326 polarity of the two main glomerular PNv classes. Despite the significant expression level,
327 *syt::GFP* appeared more scattered within LN23 dendrites and less restricted to the glomerulus
328 neuropil compared to PNv^{bi} (Fig.3B). In fact, single optical sections allow the localization of the
329 active zone marker *Brp::GFP* in LN23 dendrites outside the glomerular neuropile (Fig.3F) but
330 in PNv^{bi} confined to the V glomerulus (Fig.3G). In line with these results hemibrain EM data
331 lists enriched presynaptic site in LN23 dendrites outside the V glomerulus in contrast to the

332 restriction PNv^{bi} presynaptic sites to the glomerular neuropil (Fig.3I)
333 (https://neuprint.janelia.org/; Schlegel et al. 2021; Bates et al. 2020).

334 Following chronic sensory stimulation, PNv^{bi} showed a significant increase in the density of
335 presynaptic sites while no significant change in the amount presynaptic *syt::GFP* labeling of
336 LN23 dendrites can be observed (Fig.3D). Like the subcellular organization at ambient CO_2
337 conditions, presynaptic sites of PNv^{bi} dendrites are uniformly distributed throughout the V-
338 glomerulus (Fig.3D, last image), while most presynaptic sites of LN23 dendrites are found
339 outside of the glomerular boundaries (Fig.3D, middle image). In contrast to CO_2 relay neurons
340 PNv^{bi} and LN23, no dendritic localization of presynaptic marker transgenes could be detected
341 for PNv^{uni} (Fig.3D, first image), neither under ambient nor chronic CO_2 condition, further
342 supporting a differential synaptic profile of the two PN classes. All *syt::GFP* and
343 *DenMark::cherry* intensities were quantified using ImageJ (Fig.3H). An additional presynaptic
344 marker *syb::GFP* revealed a similar expression pattern: while PNv^{bi} showed a strong signal
345 within the glomerular boundaries, which increases following CO_2 incubation, LN23 dendrites
346 show a robust GFP signal adjacent to the neuropil border of the V glomerulus (Fig.3E). As both,
347 PNv^{bi} and PNv^{uni} are described as being excitatory, cholinergic neurons (Bates et al. 2020; Lin
348 et al. 2013; Schlegel et al. 2021; Tanaka et al. 2012) we investigated the neurotransmitter
349 identity of LN23. Anti-GABA immunostaining does not label LN23 cell bodies (Supplemental
350 Fig.3A), excluding an inhibitory function similar to canonical interglomerular LNs. These results
351 revealed not only major differences in neuronal organization among the 3 classes of CO_2 relay
352 neurons, but also a distinct response profile in intraglomerular plasticity of dendro-dendritic
353 connections. CO_2 input diverges into two more robust feed-forward channels (PNv^{uni} towards
354 LH and LN23 within the AL) while the dynamic PNv^{bi} pattern indicates intraglomerular
355 processing.

356

357 **Developmental profile of the inter-glomerular CO_2 relay neuron**
358

359 Having established the polarity of LN23, our next objective was to investigate the
360 development of this neuron, specifically focusing on how interglomerular relay neurons are
361 integrated into stereotyped antennal lobe circuits. While the glomerulus-specific assembly of
362 olfactory receptor neuron (ORN) axons with projection neuron (PN) dendrites has been

363 extensively documented (Hong & Luo 2014), less is known about the mechanisms underlying
364 the incorporation of relay neurons into these circuits. At the beginning of pupal development,
365 PN dendrites innervate the early precursor of the adult AL and occupy distinct spatial domains
366 before ORN axons enter the AL by around 20h APF (Jefferis et al. 2001; Jefferis et al. 2004).
367 LN23 neurons can be traced back to the late larval stage with a cellular morphology related to
368 SEZ (subesophageal zone) interneurons (Truman & Bate, 1988; Winding et al. 2023, Fig. 4).
369 During early pupal stages, larval LN23 precursor neurons retract from the SEZ to accumulate
370 at the ventral region of the AL precursor neuropile (Fig4A-C'). Here LN23 processes target a
371 region which is devoid of dendrites of uniglomerular PNs (Fig4F, F'). Before ORN axon arrival,
372 LN23 neurons establish a separate dendritic branch, which extends dorsally before bending
373 back to the posterior AL and merges with the main dendritic domain (Fig. 4D-E').

374 Loss of the secreted molecule *Wnt5*, which affects PN dendrite patterning (Hing et al. 2020;
375 Wu et al. 2014), leads to a continued growth of the dorsal LN23 branch along PN axon tracts
376 which exit the AL towards higher olfactory brain centers (Fig.4I-K). These results indicate that
377 LN23 neurons display an intrinsic polarity similar to uniglomerular PNs, but instead of relaying
378 sensory information from AL glomeruli to the LH/MB, a *Wnt5*-dependent mechanism seems
379 to prevent AL exit and target the presynaptic process to the extraglomerular region in the
380 ventral AL. In wild-type, ORN axons innervate the developing V glomerulus only at the
381 ipsilateral AL, in contrast to the majority of bilateral ORN classes (Fig.4F-H) (Couto et al. 2005).
382 To gain insight into the mechanisms which support glomerulus-specific ORNv input on LN23,
383 we analyzed candidate genes which are expressed on growing ORNs. Mutations in the
384 protocadherin-type cell adhesion molecule Flamingo (*fmi*), which is highly enriched on ORN
385 axons in the developing V glomerulus, affect their synaptic targeting. Here, *fmi* mutant ORNv
386 axons are no longer restricted to the glomerular boundaries but extend into the posterior AL
387 next to the output domain of LN23 (Suppl.Fig.4A, B), indicating cellular interactions to restrict
388 class-specific axon-dendrite recognition within the glomerular domain.

389 In summary, despite being morphologically classified as a local interneuron, the LN23 class
390 shows cellular and developmental features similar to those of olfactory projection neurons: a
391 highly polarized neuronal morphology in the adult olfactory system is established by a
392 glomerulus-specific dendrite targeting for singular ORN input and a default axonal extension
393 along olfactory PN tracts rerouted by external signals (Komiyama & Luo, 2006).

394 **LN23 mediates CO_2-induced aversion**
395

396 To test the role of the different CO_2 relay neurons on *Drosophila* behavior, we expressed the
397 *shibire^{ts}* transgene to block synaptic transmission in a cell type specific manner (Chen et al.
398 1991; Kitamoto 2001). Neuronal silencing of each of the two glomerular PNs led to a reduction
399 of innate CO_2 avoidance, with stronger effects observed for PNv^{uni} compared to PNv^{bi} (Fig. 5A).
400 While CO_2 avoidance can still be observed following the neuronal silencing of each PN class,
401 *shibire^{ts}* induced silencing of LN23 fully abolished aversion behavior towards CO_2 (Fig. 5A). To
402 test for cell type specificity of the behavioral phenotype following LN23 silencing, we used the
403 Ca^{2+} dependent LexA activation of the CaLexA construct for shi^{ts} expression and observed a
404 reduction of the innate CO_2 aversion (Fig. 5B) (Masuyama et al. 2012). To increase lexA levels
405 we chronically exposed flies to high levels of CO_2. Interestingly, increased CaLexA mediated
406 shi^{ts} expression via chronic exposure not only suppressed behavioral aversion but led to a
407 significant level of attraction towards CO_2 (Fig.5B). These results indicate a prominent function
408 of LN23 in CO_2 valence coding: Blocking LN23 activity is sufficient to fully suppress CO_2-induced
409 behavioral aversion and together with the GABAergic suppression of PNv^{bi} during habituation
410 an attraction towards CO_2 is observed, which phenocopies the silencing of ORNv (Jones et al.
411 2007; Kwon et al. 2007, MacWilliam et al. 2018; Suh et al. 2004).

412 To further determine if these relay neurons are sufficient for behavioral aversion, we
413 optogenetically activated each neuron type and measured the behavioral response (Inagaki
414 et al. 2014; Klapoetke et al. 2014; Pulver et al. 2009) (see M&M). Light-induced activation of
415 ORNv (*GR21a-Gal4*) expressing UAS-ReaCh led to strong aversion (Fig. 5C). Similarly,
416 optogenetic activation of LN23 is sufficient to trigger behavioral aversion via two independent
417 Gal4 driver lines (LN23 Gal4 and the alternative line we used: VT48408-Gal4; Fig.5C) or by $Ca2^{+}$
418 induced LexA activation (Fig.5D). In contrast, no change in light-induced activation for both
419 PNv^{bi} (two independent driver lines, see Methods) nor PNv^{uni} could be observed (Fig.5C).
420 These results support a predominant role of LN23 in CO_2-induced avoidance behavior.
421 Compared to the more dynamic activity of PNv^{bi} following acute and chronic sensory
422 stimulation, LN23 shows little changes in intrinsic activity, representing ORNv activity
423 independent of changes in CO_2 levels or temporal pattern. Based on these findings we propose
424 a ground state of ORNv/LN23 mediated aversion induced by ambient CO_2 default state, which
425 is modified either by the parallel PN channels or downstream of LN23.

426 **Third-order neurons postsynaptic to LN23 have a putative role in valence coding**
427

428 To gain further insights into the unique organization of the LN23 pathway compared to the
429 glomerular relay channel, we analyzed the postsynaptic candidate neurons within the
430 posterior AL. Two PN types, l2_PNm17 and sm_PNm1 are receiving a large proportion of their
431 synaptic input (27% and 18%, respectively) from LN23 (Fig.6A, neuPrint, Janelia Research
432 Campus; https://neuprint.janelia.org/; Schlegel et al. 2021). Like the two PN classes of the V
433 glomerulus, PNm1 and PNm17 show distinct relay properties: While input into PNm1 is mostly
434 restricted to the LN23-CO_2 channel, dendrites of PNm17 extend into adjacent VP1 and VP3-5
435 glomeruli to receive direct input from thermo- and humidity- receptor neurons (neuPrint,
436 Janelia Research Campus; https://neuprint.janelia.org/; Frank et al. 2015; Marin et al. 2020).
437 Both types of non-olfactory relay neurons target multiple distinct brain areas adjacent to the
438 canonical olfactory LH, the posterior lateral protocerebrum (PLP), superior clamp (SCL) and
439 the superior lateral protocerebrum (SLP) (Fig6 A, B, C) (Ito et al. 2014). To visualize the
440 trajectories of the PNs, we used MCFO (Aso et al. 2014) to create single cell clones, which
441 show that PNm1 and PNm17 axons turn close before entering the LH to target adjacent brain
442 regions (Fig. 6B, C). Of note, compared to glomerular PNv^{uni} and PNv^{bi}, PNm1 and PNm17
443 receive only minor input from GABAergic LNs (neuPrint, Janelia Research Campus;
444 https://neuprint.janelia.org/), indicating reduced gain control properties of the extra-
445 glomerular ORN→LN23→PNm pathway (Olsen & Wilson, 2008).

446 Optogenetic activation of each of the two PNm class neurons downstream of LN23 induce
447 opposite behavioral responses: While activity of the "CO_2-only" class PNm1 results in strong
448 aversion, the "multi-modal" PNm17 initiates behavioral attraction (Fig.6D). Furthermore, CO_2-
449 induced aversive behavior could be attenuated following shi^{ts}-mediated silencing of PNm1 but
450 was not changed by silencing PNm17 (Fig.6 E, F). Interestingly, FlyWire.ai (Dorkenwald et al.
451 2024; Eckstein et al. 2024; Schlegel et al. 2024; Zheng et al. 2018) revealed distinct
452 neurotransmitter identities for the two PNm classes, GABA expression for PNm1, while PNm17
453 shows a cholinergic synaptic profile. Together with the behavioral responses following
454 optogenetic activation this suggests a circuit motif in which the default activity of the
455 ORNv→LN23→PNm1 channel by ambient CO_2 sensation blocks a central brain region
456 important for the generation of behavioral attraction (Dolan et al. 2019).

457

458 **Connectivity in higher brain centers and lateral communication in the antennal lobe**
459

460 As the glomerular PNs and the extra-glomerular LN23→PNm channels target adjacent central
461 brain regions we asked whether the two parallel CO_2 pathways converge onto common
462 downstream neurons. The hemibrain dataset (https://neuprint.janelia.org/; Plaza et al. 2022;
463 Scheffer et al. 2020) identified three main types of glutamatergic LH neurons (FlyWire.ai;
464 Dorkenwald et al. 2024; Eckstein et al. 2024; Schlegel et al. 2024; Zheng et al. 2018) as PNv or
465 PNm targets: LH^{PD5c1} as the primary target of PNv^{bi} (Fig.6 G), LH^{PV9b1} downstream of PNm1
466 (Fig.6 H) and LH^{CENT4} as the major postsynaptic partner of PNv^{uni} (Fig.6 I). All 3 LH target
467 neurons of the parallel CO_2 pathways are directly interconnected (Fig. 8): While LH^{PV9b1} not
468 only receives input from PNm1 but also from PNv^{bi}, LH^{PD5c1}, the main downstream target of
469 PNv^{bi}, is also targeted by LH^{CENT4}, the primary postsynaptic partner of PNv^{uni}. This core motif
470 of CO_2 perception receives additional input from other sensory modalities. LH^{PD5c1} gains input
471 from "food-sensing" glomeruli (DM4, DC4/DP1, and VM7) via class-specific cholinergic PNs,
472 indicating a neuronal integrator of CO_2 and food-related cues (Couto et al. 2005; Dumenil et
473 al. 2025; Min et al. 2013). In addition, LH^{CENT4} is also a main target for $l2PN^{VP4+VL1}$, mediating
474 the perception of dryness and pyrrolidine-type odorants, thereby adding another layer of
475 multi-modal sampling to the LN23 → PNm1 pathway (Fig.8) (Li et al. 2022; Choi et al. 2022; Ni
476 2021). Interestingly, the convergence of the glomerular CO_2 and food channels is not only
477 observed for LH neurons downstream of AL relay pathways but seems to occur already at the
478 level of AL glomeruli. Hemibrain describes with l2LN19 another class of polarized local
479 interneuron (Fig.7A, B) with enriched postsynaptic sites at "food-sensing" glomeruli DM4,
480 DC4/DP1, and VM7 (Fig.7A) as well as targeted output onto PNv^{bi} and PNv^{uni} in the V-
481 glomerulus (Fig.7B), but merely with LN23 (Fig.7C) (https://neuprint.janelia.org/; Schlegel et
482 al. 2021; Bates et al.2020). Accordingly, optogenetic activation of LN19 led to an aversive
483 behavioral response (Fig.7D), while inhibition had no effect (Fig.7E).

484 Based on these distinct connectivity patterns and behavioral response profiles of individual
485 relay neurons we are proposing the following circuit mechanism for CO_2 valence coding (Fig.8):
486 The activity of CO_2-responsive sensory neurons (ORNv, black) is relayed by parallel PN
487 channels and converge onto two central brain target neurons of opposite intrinsic valence
488 identity. The glomerular PNs target the ventral domain of LH^{PD5} to trigger behavioral aversion
489 and extraglomerular PNs activated via the lateral LN23 relay converge onto LH^{PV9} which

490 mediates attraction. While PNm17 supports LH^{PV9} activity, GABAergic PNm1 blocks LH^{PV9}
491 through which the negative valence state of LH^{PD5} triggers avoidance. This core aversion
492 pathway (PNv^{bi}/PNv^{uni}/PNm1), without prominent GABAergic modulation, directly represents
493 the activity of CO_2 sensory neurons, is modified either via the activation of the dorsal LH^{PD5}
494 domain by fruit odor PNs ($PN^{DM/VM/DC}$) or by an increase of PNm17 through non-olfactory
495 sensory neurons to support a context-dependent behavioral response repertoire.

496 **Discussion**
497

498 In *Drosophila*, the activation of a single class of CO_2 receptive sensory neurons induces
499 avoidance behavior, which is modified by multiple external and internal stimuli (Bräcker et al.
500 2013; Faucher et al. 2006; Dissegna et al. 2021; Suh et al. 2004; Turner and Ray, 2009). How
501 does the *Drosophila* brain transform ORNv input into flexible behavioral responses towards
502 CO_2? Here we identified a novel CO_2 relay channel with unique morphological and
503 physiological properties compared to the canonical glomerular PN pathway. First, instead of
504 direct transmission of sensory input by glomerular PNs in the anterior AL towards higher brain
505 centers, the ORNv induced activation of the local interneuron LN23 relays peripheral CO_2
506 sensation to an extraglomerular neuropil of the posterior AL generating two parallel output
507 channels with different target areas. Second, in contrast to the high level of neuronal plasticity
508 observed for PNs within glomerular circuits, LN23 analysis revealed very little dynamic
509 changes under different physiological conditions. This might be due to distinct intrinsic
510 features of PNs and LN23 such as the expression of ion channels or receptor molecules but
511 could also be explained by the absence of glomerular GABAergic neurons at the
512 extraglomerular CO_2 pathway. Third, following the manipulation of neuronal activity, only
513 LN23, but no individual PNs are able to induce an aversive behavioral response similar to
514 ORNv. Finally, the extraglomerular CO_2 pathway includes a structural segregation of opposite
515 valence-encoding elements, in which the "CO_2-only" neuron induces aversion while activation
516 of the parallel "multi-modal" channel determines behavioral attraction. These findings are
517 consistent with a designated circuit motif encoding a default behavioral state of avoidance
518 even under atmospheric CO_2 levels. As the "CO_2-only" relay neuron PNm1 has a predicted
519 GABAergic identity (FlyWire.ai; Dorkenwald et al. 2024; Eckstein et al. 2024; Schlegel et al.
520 2024; Zheng et al. 2018), the previously reported ORNv induced avoidance (MacWilliam et al.

521 2018; Das et al. 2011) could be explained with the inhibition of a premotor area by the LN23
522 channel.

523 The interplay between the extraglomerular default channel and the glomerular dynamic
524 pathway in encoding behavioral avoidance was demonstrated in the context of habituation.
525 While the increased GABAergic inhibition of glomerular PNs following chronic CO_2 sensation
526 reduces innate aversion, the simultaneous silencing of LN23 not only eliminates all aversive
527 response features but reverses CO_2 valence to trigger attraction. Interestingly, the reduced
528 aversion through inhibition of PN activity in the context of habituation seems partially
529 compensated by increasing PNv^{bi} synaptic plasticity. We observed a strong gain of presynaptic
530 sites of glomerular PNv^{bi} dendrites onto LN23, which might maintain a balanced level of
531 aversion activity for local CO_2 levels following habituation (Das et al. 2011; Sachse et al. 2007).
532 Although both PNv^{uni} and PNv^{bi} are excitatory cholinergic projection neurons (Tanaka et al.
533 2012; Lin et al. 2013; Bates et al. 2020; Schlegel et al. 2021), they differ in their cellular
534 organization and behavioral function. In contrast to PNv^{bi}, PNv^{uni} dendrites lack presynaptic
535 sites, therefore specifies a feed-forward channel similar to LN23. Based on these results we
536 are proposing complementary function of the three relay neurons in mediating flexible CO_2
537 behavioral response patterns: While LN23 encodes default avoidance under ambient
538 conditions, supported by PNv^{uni} as a sensor for elevated local levels of CO_2, PNv^{bi} defines the
539 main component of experience-dependent modulation by LNs and neurons of the MB calyx
540 (CA) (Bräcker et al. 2013).

541 Interestingly, developmental analysis revealed a polarized growth pattern of LN23 that
542 resembles projection neurons more than typical local interneurons (Jefferis et al. 2004;
543 Komiyama & Luo 2006). LN23 originates from a larval interneuron located in the
544 suboesophageal zone (SEZ), which undergoes remodeling into an adult olfactory interneuron
545 during early pupal stages (Truman & Bate, 1988). We hypothesize that the secreted *Wnt5*
546 protein, a critical factor for initial projection neuron dendrite patterning, supports the
547 targeting of LN23 processes to the posterior antennal lobe (AL) region. Like the genetically
548 defined recognition mechanisms that guide glomerulus-specific ORN-PN connectivity, growing
549 ORNv axons appear to target LN23 dendrites as synaptic partners. Since LN23 dendrites are
550 organized into a defined glomerular input and extraglomerular output zone, we propose

551 Flamingo-dependent expression on ingrowing ORN axons to prevent sensory input to LN23
552 outside the glomerular domain.

553 The divergence of CO_2-induced ORN activation into parallel relay channels allows for early
554 convergence of additional sensory information. This includes not only the integration of non-
555 olfactory cues by the positive valence branch PNm17 downstream of LN23 (Frank et al. 2015;
556 Li et al. 2022), but also the sampling of food-odor-sensitive glomeruli by the polarized
557 interneuron LN19 for V-glomerulus input (Couto et al. 2005; Dumenil et al. 2025; Min et al.
558 2013). The convergence of different parallel CO_2 channels onto a common set of lateral horn
559 (LH) interneurons suggests a potential hub for motor action control (Dolan et al. 2019). The
560 results presented in this study support a conceptual model in which the default state of
561 behavioral aversion, induced through inhibition of an LH motor hub by the "CO_2-only"
562 ORNv→LN23→PNm1 pathway, is modified by the inclusion of additional glomerular and
563 extraglomerular projection neuron classes to allow approach behavior. Further studies on the
564 physiological architecture of the CO_2 core circuit within and downstream of the LH may reveal
565 deeper insights into the multi-modal processing underlying flexible, context-dependent
566 behaviors.

567 Additionally, despite the conserved molecular receptor identity of CO_2 sensory neurons
568 among insects, species-specific behavioral responses to local CO_2 concentrations are evident
569 (Turner & Ray 2009). In many species, such as mosquitoes, elevated CO_2 levels signal potential
570 food sources and elicit an attractive response (Tauxe et al. 2013; Siju 2009; Ghaninia 2007).
571 The identification of a dedicated CO_2 aversion channel in *D. melanogaster* opens new avenues
572 for comparative research into circuit motifs and provides insight into the neural basis of
573 behavioral flexibility across insect evolution (Oram & Card 2022).

574

575

576

577

578

References

Aso, Y., Hattori, D., Yu, Y., Johnston, R. M., Iyer, N. A., Ngo, T. T., Dionne, H., Abbott, L. F., Axel, R., Tanimoto, H., & Rubin, G. M. (2014). The neuronal architecture of the mushroom body provides a logic for associative learning. *eLife*, *3*, e04577. https://doi.org/10.7554/eLife.04577

Bates, A. S., Schlegel, P., Roberts, R. J. V., Drummond, N., Tamimi, I. F. M., Turnbull, R., Zhao, X., Marin, E. C., Popovici, P. D., Dhawan, S., Jamasb, A., Javier, A., Serratosa Capdevila, L., Li, F., Rubin, G. M., Waddell, S., Bock, D. D., Costa, M., & Jefferis, G. S. X. E. (2020). Complete Connectomic Reconstruction of Olfactory Projection Neurons in the Fly Brain. *Current biology : CB*, *30*(16), 3183–3199.e6. https://doi.org/10.1016/j.cub.2020.06.042

Bräcker, L. B., Siju, K. P., Varela, N., Aso, Y., Zhang, M., Hein, I., Vasconcelos, M. L., & Grunwald Kadow, I. C. (2013). Essential role of the mushroom body in context-dependent CO_2 avoidance in Drosophila. *Current biology : CB*, *23*(13), 1228–1234. https://doi.org/10.1016/j.cub.2013.05.029

Das Chakraborty, S., Chang, H., Hansson, B. S., & Sachse, S. (2022). Higher-order olfactory neurons in the lateral horn support odor valence and odor identity coding in *Drosophila*. *eLife*, *11*, e74637. https://doi.org/10.7554/eLife.74637

Chen, M. S., Obar, R. A., Schroeder, C. C., Austin, T. W., Poodry, C. A., Wadsworth, S. C., & Vallee, R. B. (1991). Multiple forms of dynamin are encoded by shibire, a Drosophila gene involved in endocytosis. *Nature*, *351*(6327), 583–586. https://doi.org/10.1038/351583a0

Choi, K., Kim, W. K., & Hyeon, C. (2022). Olfactory responses of *Drosophila* are encoded in the organization of projection neurons. *eLife*, *11*, e77748. https://doi.org/10.7554/eLife.77748

Couto, A., Alenius, M., & Dickson, B. J. (2005). Molecular, anatomical, and functional organization of the Drosophila olfactory system. *Current biology : CB*, *15*(17), 1535–1547. https://doi.org/10.1016/j.cub.2005.07.034

Das, S., Sadanandappa, M. K., Dervan, A., Larkin, A., Lee, J. A., Sudhakaran, I. P., Priya, R., Heidari, R., Holohan, E. E., Pimentel, A., Gandhi, A., Ito, K., Sanyal, S., Wang, J. W., Rodrigues, V., & Ramaswami, M. (2011). Plasticity of local GABAergic interneurons drives olfactory habituation. *Proceedings of the National Academy of Sciences of the United States of America*, *108*(36), E646–E654. https://doi.org/10.1073/pnas.1106411108

Dissegna, A., Turatto, M., & Chiandetti, C. (2021). Context-Specific Habituation: A Review. *Animals : an open access journal from MDPI*, *11*(6), 1767. https://doi.org/10.3390/ani11061767

Dolan, M. J., Frechter, S., Bates, A. S., Dan, C., Huoviala, P., Roberts, R. J. V., Schlegel, P., Dhawan, S., Tabano, R., Dionne, H., Christoforou, C., Close, K., Sutcliffe, B., Giuliani, B., Feng, L., Costa, M., Ihrke, G., Meissner, G. W., Bock, D. D., Aso, Y., Rubin, G. M., & Jefferis, G. S. X. E. (2019). Neurogenetic dissection of the Drosophila lateral horn reveals major outputs, diverse behavioural functions, and interactions with the mushroom body. *eLife, 8*, e43079. https://doi.org/10.7554/eLife.43079

Dorkenwald, S., Matsliah, A., Sterling, A. R., Schlegel, P., Yu, S. C., McKellar, C. E., Lin, A., Costa, M., Eichler, K., Yin, Y., Silversmith, W., Schneider-Mizell, C., Jordan, C. S., Brittain, D., Halageri, A., Kuehner, K., Ogedengbe, O., Morey, R., Gager, J., Kruk, K., … FlyWire Consortium (2024). Neuronal wiring diagram of an adult brain. *Nature*, *634*(8032), 124–138. https://doi.org/10.1038/s41586-024-07558-y

Dumenil, C., Yildirim, G., & Haase, A. (2025). Differential Coding of Fruit, Leaf, and Microbial Odours in the Brains of *Drosophila suzukii* and *Drosophila melanogaster*. *Insects*, *16*(1), 84. https://doi.org/10.3390/insects16010084

Eckstein, N., Bates, A. S., Champion, A., Du, M., Yin, Y., Schlegel, P., Lu, A. K., Rymer, T., Finley-May, S., Paterson, T., Parekh, R., Dorkenwald, S., Matsliah, A., Yu, S. C., McKellar, C., Sterling, A., Eichler, K., Costa, M., Seung, S., Murthy, M., … Funke, J. (2024). Neurotransmitter classification from electron microscopy images at synaptic sites in Drosophila melanogaster. *Cell*, *187*(10), 2574–2594.e23. https://doi.org/10.1016/j.cell.2024.03.016

636 **Faucher, C., Forstreuter, M., Hilker, M., & de Bruyne, M. (2006).** Behavioral responses of
637 Drosophila to biogenic levels of carbon dioxide depend on life-stage, sex and olfactory
638 context. *The Journal of experimental biology*, *209*(Pt 14), 2739–2748.
639 https://doi.org/10.1242/jeb.02297

640 **Frank, D. D., Jouandet, G. C., Kearney, P. J., Macpherson, L. J., & Gallio, M. (2015).**
641 Temperature representation in the Drosophila brain. *Nature*, *519*(7543), 358–361.
642 https://doi.org/10.1038/nature14284

643 **Frechter, S., Bates, A. S., Tootoonian, S., Dolan, M. J., Manton, J., Jamasb, A. R., Kohl, J.,**
644 **Bock, D. D., & Jefferis, G. S. X. E. (2019).** Functional and anatomical specificity in a higher
645 olfactory centre. *eLife*, 8, e44590. https://doi.org/10.7554/eLife.44590

646 **Ghaninia, M. (2007).** *Olfaction in Mosquitoes.* Doctoral Thesis, Swedish University of
647 Agricultural Sciences. https://pub.epsilon.slu.se/1560/.

648 **Grabe, V., Baschwitz, A., Dweck, H. K. M., Lavista-Llanos, S., Hansson, B. S., & Sachse, S.**
649 **(2016).** Elucidating the neuronal architecture of olfactory glomeruli in the Drosophila antennal
650 lobe. *Cell Reports*, 16(12), 3401–3413. https://doi.org/10.1016/j.celrep.2016.08.063

651 **Hansson, B. S., & Stensmyr, M. C. (2011).** Evolution of insect olfaction. *Neuron, 72*(5), 698–
652 711. https://doi.org/10.1016/j.neuron.2011.11.003

653 **Hing, H., Reger, N., Snyder, J., & Fradkin, L. G. (2020).** Interplay between axonal Wnt5-Vang
654 and dendritic Wnt5-Drl/Ryk signaling controls glomerular patterning in the Drosophila
655 antennal lobe. *PLoS genetics*, *16*(5), e1008767.
656 https://doi.org/10.1371/journal.pgen.1008767

657 **Hong, W., & Luo, L. (2014).** Genetic control of wiring specificity in the fly olfactory system.
658 *Genetics*, 196(1), 17–29. https://doi.org/10.1534/genetics.113.154336

659 **Inagaki, H. K., Jung, Y., Hoopfer, E. D., Wong, A. M., Mishra, N., Lin, J. Y., Tsien, R. Y., &**
660 **Anderson,D.J.(2014).** Optogenetic control of *Drosophila* using a red-shifted channelrhodopsin
661 (ReaChR). *Nature Methods, 11*(3), 325–332. https://doi.org/10.1038/nmeth.2765

662

Ito, K., Shinomiya, K., Ito, M., Armstrong, J. D., Boyan, G., Hartenstein, V., Harzsch, S., Heisenberg, M., Homberg, U., Jenett, A., Keshishian, H., Restifo, L. L., Rössler, W., Simpson, J. H., Strausfeld, N. J., Strauss, R., Vosshall, L. B., & Insect Brain Name Working Group (2014). A systematic nomenclature for the insect brain. *Neuron*, *81*(4), 755–765. https://doi.org/10.1016/j.neuron.2013.12.017

Jefferis, G. S., Marin, E. C., Stocker, R. F., & Luo, L. (2001). Target neuron prespecification in the olfactory map of Drosophila. *Nature*, *414*(6860), 204–208. https://doi.org/10.1038/35102574

Jefferis, G. S., Vyas, R. M., Berdnik, D., Ramaekers, A., Stocker, R. F., Tanaka, N. K., Ito, K., & Luo, L. (2004). Developmental origin of wiring specificity in the olfactory system of Drosophila. *Development (Cambridge, England)*, *131*(1), 117–130. https://doi.org/10.1242/dev.00896

Jones, W. D., Cayirlioglu, P., Kadow, I. G., & Vosshall, L. B. (2007). Two chemosensory receptors together mediate carbon dioxide detection in *Drosophila*. *Nature*, 445(7123), 86–90. https://doi.org/10.1038/nature05466

Kitamoto T. (2001). Conditional modification of behavior in Drosophila by targeted expression of a temperature-sensitive shibire allele in defined neurons. *Journal of neurobiology*, *47*(2), 81–92. https://doi.org/10.1002/neu.1018

Kittel, R. J., Wichmann, C., Rasse, T. M., Fouquet, W., Schmidt, M., Schmid, A., Wagh, D. A., Pawlu, C., Kellner, R. R., Willig, K. I., Hell, S. W., Buchner, E., Heckmann, M., & Sigrist, S. J. (2006). Bruchpilot promotes active zone assembly, Ca2+ channel clustering, and vesicle release. *Science (New York, N.Y.)*, *312*(5776), 1051–1054. https://doi.org/10.1126/science.1126308

Klapoetke, N. C., Murata, Y., Kim, S. S., Pulver, S. R., Birdsey-Benson, A., Cho, Y. K., Morimoto, T. K., Chuong, A. S., Carpenter, E. J., Tian, Z., Wang, J., Xie, Y., Yan, Z., Zhang, Y., Chow, B. Y., Surek, B., Melkonian, M., Jayaraman, V., Constantine-Paton, M., Wong, G. K., … Boyden, E. S. (2014). Independent optical excitation of distinct neural populations. *Nature methods*, *11*(3), 338–346. https://doi.org/10.1038/nmeth.2836

691 **Komiyama, T., & Luo, L. (2006).** Development of wiring specificity in the olfactory
692 system. *Current opinion in neurobiology*, *16*(1), 67–73.
693 https://doi.org/10.1016/j.conb.2005.12.002

694 **Koyama, T., Rodrigues, M. A., Athanasiadis, A., Shingleton, A. W., & Mirth, C. K. (2021).**
695 A nutrient-responsive hormonal circuit mediates an inter-organ growth coordination in
696 *Drosophila*.*Nature Communications, 12*, 7168.
697 https://doi.org/10.1038/s41467-021-25445-2

698 **Kwon, J. Y., A. Dahanukar, L. A. Weiss, and J. R. Carlson. (2007).** The Molecular Basis of CO_2
699 Reception in Drosophila. *Proceedings of the National Academy of Sciences USA* 104 (9): 3574–
700 78. https://doi.org/10.1073/pnas.0700079104.

701 **Lewis, L. P. C., Siju, K. P., Aso, Y., Friedrich, A. B., Bulteel, A. J. B., Rubin, G. M., & Grunwald**
702 **Kadow, I. C. (2015).** A higher brain circuit for immediate integration of conflicting sensory
703 information in *Drosophila*. *Current Biology, 25*(17), 2203–2214.
704 https://doi.org/10.1016/j.cub.2015.07.015

705 **Li, S., Li, B., Gao, L., Wang, J., & Yan, Z. (2022).** Humidity response in Drosophila olfactory
706 sensory neurons requires the mechanosensitive channel TMEM63. *Nature*
707 *communications*, *13*(1), 3814. https://doi.org/10.1038/s41467-022-31253-z

708 **Lin, H. H., Chu, L. A., Fu, T. F., Dickson, B. J., & Chiang, A. S. (2013).** Parallel neural pathways
709 mediate CO_2 avoidance responses in Drosophila. *Science (New York, N.Y.)*, *340*(6138), 1338–
710 1341. https://doi.org/10.1126/science.1236693

711 **Liou, N. F., Lin, S. H., Chen, Y. J., Tsai, K. T., Yang, C. J., Lin, T. Y., Wu, T. H., Lin, H. J., Chen, Y.**
712 **T., Gohl, D. M., Silies, M., & Chou, Y. H. (2018).** Diverse populations of local interneurons
713 integrate into the Drosophila adult olfactory circuit. *Nature communications*, *9*(1), 2232.
714 https://doi.org/10.1038/s41467-018-04675-x

715 **Macpherson, L. J., Zaharieva, E. E., Kearney, P. J., Alpert, M. H., Lin, T. Y., Turan, Z., Lee, C.**
716 **H., & Gallio, M. (2015).** Dynamic labelling of neural connections in multiple colours by trans-
717 synaptic fluorescence complementation. *Nature communications*, *6*, 10024.
718 https://doi.org/10.1038/ncomms10024

MacWilliam, D., J. Kowalewski, A. Kumar, C. Pontrello, and A. Ray. (2018). Signaling Mode of the Broad-Spectrum Conserved CO_2 Receptor Is One of the Important Determinants of Odor Valence in Drosophila. *Neuron* 97 (5): 1153–67.e4. https://doi.org/10.1016/j.neuron.2018.01.028.

Marin, E. C., Büld, L., Theiss, M., Sarkissian, T., Roberts, R. J. V., Turnbull, R., Tamimi, I. F. M., Pleijzier, M. W., Laursen, W. J., Drummond, N., Schlegel, P., Bates, A. S., Li, F., Landgraf, M., Costa, M., Bock, D. D., Garrity, P. A., & Jefferis, G. S. X. E. (2020). Connectomics Analysis Reveals First-, Second-, and Third-Order Thermosensory and Hygrosensory Neurons in the Adult Drosophila Brain. *Current biology : CB*, *30*(16), 3167–3182.e4. https://doi.org/10.1016/j.cub.2020.06.028

Masuyama, K., Zhang, Y., Rao, Y., & Wang, J. W. (2012). Mapping neural circuits with activity-dependent nuclear import of a transcription factor. *Journal of neurogenetics*, *26*(1), 89–102. https://doi.org/10.3109/01677063.2011.642910

Min, S., Ai, M., Shin, S. A., & Suh, G. S. (2013). Dedicated olfactory neurons mediating attraction behavior to ammonia and amines in Drosophila. *Proceedings of the National Academy of Sciences of the United States of America*, *110*(14), E1321–E1329. https://doi.org/10.1073/pnas.1215680110

Nagel, K. I., & Wilson, R. I. (2016). Mechanisms underlying population response dynamics in inhibitory interneurons of the *Drosophila* antennal lobe. *Journal of Neuroscience, 36*(14), 4325–4338. https://doi.org/10.1523/JNEUROSCI.3887-15.2016

Nern, A., Pfeiffer, B. D., & Rubin, G. M. (2015). Optimized tools for multicolor stochastic labeling reveal diverse stereotyped cell arrangements in the fly visual system. *PNAS*, 112(22), E2967–E2976. https://doi.org/10.1073/pnas.1506763112

Ni L. (2021). The Structure and Function of Ionotropic Receptors in *Drosophila*. *Frontiers in molecular neuroscience*, *13*, 638839. https://doi.org/10.3389/fnmol.2020.638839

Nicolaï, L. J., Ramaekers, A., Raemaekers, T., Drozdzecki, A., Mauss, A. S., Yan, J., Landgraf, M., Annaert, W., & Hassan, B. A. (2010). Genetically encoded dendritic marker sheds light on neuronal connectivity in Drosophila. *Proceedings of the National Academy of Sciences of the United States of America*, *107*(47), 20553–20558. https://doi.org/10.1073/pnas.1010198107

Olsen, S. R., & Wilson, R. I. (2008). Lateral presynaptic inhibition mediates gain control in an olfactory circuit. *Nature*, *452*(7190), 956–960. https://doi.org/10.1038/nature06864

Oram, T. B., & Card, G. M. (2022). Context-dependent control of behavior in Drosophila. *Current opinion in neurobiology*, *73*, 102523. https://doi.org/10.1016/j.conb.2022.02.003

Plaza, S. M., Clements, J., Dolafi, T., Umayam, L., Neubarth, N. N., Scheffer, L. K., & Berg, S. (2022). *neu*Print: An open access tool for EM connectomics. *Frontiers in neuroinformatics*, *16*, 896292. https://doi.org/10.3389/fninf.2022.896292

Pulver, S. R., Pashkovski, S. L., Hornstein, N. J., Garrity, P. A., & Griffith, L. C. (2009). Temporal dynamics of neuronal activation by Channelrhodopsin-2 and TRPA1 determine behavioral output in *Drosophila* larvae. *Journal of Neurophysiology, 101*(6), 3075–3088. https://doi.org/10.1152/jn.00071.2009

Root, C. M., Masuyama, K., Green, D. S., Enell, L. E., Nässel, D. R., Lee, C. H., & Wang, J. W. (2008). A presynaptic gain control mechanism fine-tunes olfactory behavior. *Neuron*, *59*(2), 311–321. https://doi.org/10.1016/j.neuron.2008.07.003

Sachse, S., & Beshel, J. (2016). The good, the bad, and the hungry: how the central brain codes odor valence to facilitate food approach in Drosophila. *Current opinion in neurobiology*, *40*, 53–58. https://doi.org/10.1016/j.conb.2016.06.012

Sachse, S., Rueckert, E., Keller, A., Okada, R., Tanaka, N. K., Ito, K., & Vosshall, L. B. (2007). Activity-dependent plasticity in an olfactory circuit. *Neuron*, *56*(5), 838–850. https://doi.org/10.1016/j.neuron.2007.10.035

Sadanandappa, M. K., Redondo, B. B., Michels, B., Rodrigues, V., Gerber, B., VijayRaghavan, K., Buchner, E., & Ramaswami, M. (2013). Synapsin function in GABA-ergic interneurons is required for short-term olfactory habituation. *Journal of Neuroscience, 33*(42), 16576–16585. https://doi.org/10.1523/JNEUROSCI.3142-13.2013

775 **Scheffer, L. K., Xu, C. S., Januszewski, M., Lu, Z., Takemura, S. Y., Hayworth, K. J., Huang, G.**
776 **B., Shinomiya, K., Maitlin-Shepard, J., Berg, S., Clements, J., Hubbard, P. M., Katz, W. T.,**
777 **Umayam, L., Zhao, T., Ackerman, D., Blakely, T., Bogovic, J., … Meinertzhagen, I. A. (2020).**
778 A connectome and analysis of the adult Drosophila central brain. *eLife, 9*, e57443.
779 https://doi.org/10.7554/eLife.57443

780 **Schlegel, P., Bates, A. S., Stürner, T., Jagannathan, S. R., Drummond, N., Hsu, J., Serratosa**
781 **Capdevila, L., Javier, A., Marin, E. C., Barth-Maron, A., Tamimi, I. F., Li, F., Rubin, G. M., Plaza,**
782 **S. M., Costa, M., & Jefferis, G. S. X. E. (2021).** Information flow, cell types and stereotypy in a
783 full olfactory connectome. *eLife*, *10*, e66018. https://doi.org/10.7554/eLife.66018

784 **Schlegel, P., Yin, Y., Bates, A. S., Dorkenwald, S., Eichler, K., Brooks, P., Han, D. S., Gkantia,**
785 **M., Dos Santos, M., Munnelly, E. J., Badalamente, G., Serratosa Capdevila, L., Sane, V. A.,**
786 **Fragniere, A. M. C., Kiassat, L., Pleijzier, M. W., Stürner, T., Tamimi, I. F. M., Dunne, C. R.,**
787 **Salgarella, I., … Jefferis, G. S. X. E. (2024).** Whole-brain annotation and multi-connectome cell
788 typing of Drosophila. *Nature*, *634*(8032), 139–152. https://doi.org/10.1038/s41586-024-
789 07686-5

790 **Semelidou, O., Acevedo, S. F., & Skoulakis, E. M. (2018).** Temporally specific engagement of
791 distinct neuronal circuits regulating olfactory habituation in *Drosophila*. *eLife*, *7*, e39569.
792 https://doi.org/10.7554/eLife.39569

793 **Shearin, H. K., Quinn, C. D., Mackin, R. D., Macdonald, I. S., & Stowers, R. S. (2018).** t-GRASP,
794 a targeted GRASP for assessing neuronal connectivity. *Journal of neuroscience methods*, *306*,
795 94–102. https://doi.org/10.1016/j.jneumeth.2018.05.014

796 **Siju, K. P. (2009).** *Neuromodulation in the Chemosensory System of Mosquitoes:*
797 *Neuroanatomy and Physiology.* Doctoral Thesis, Swedish University of Agricultural Sciences.
798 https://pub.epsilon.slu.se/1956/.

799 **Suh, G. S., Wong, A. M., Hergarden, A. C., Wang, J. W., Simon, A. F., Benzer, S., Axel, R., &**
800 **Anderson, D. J. (2004).** A single population of olfactory sensory neurons mediates an innate
801 avoidance behaviour in Drosophila. *Nature*, *431*(7010), 854–859.
802 https://doi.org/10.1038/nature02980

Tanaka, N. K., Endo, K., & Ito, K. (2012). Organization of antennal lobe-associated neurons in adult Drosophila melanogaster brain. *The Journal of comparative neurology*, *520*(18), 4067–4130. https://doi.org/10.1002/cne.23142

Tauxe, G. M., MacWilliam, D., Boyle, S. M., Guda, T., & Ray, A. (2013). Targeting a dual detector of skin and CO2 to modify mosquito host seeking. *Cell*, *155*(6), 1365–1379. https://doi.org/10.1016/j.cell.2013.11.013

Truman, James W., and Michael Bate. (1988). Spatial and Temporal Patterns of Neurogenesis in the Central Nervous System of *Drosophila melanogaster*. *Developmental Biology* 125 (1): 145–57.

Turner, S. L., & Ray, A. (2009). Modification of CO_2 avoidance behaviour in Drosophila by inhibitory odorants. *Nature*, *461*(7261), 277–281. https://doi.org/10.1038/nature08295

van Breugel, F., Huda, A., & Dickinson, M. H. (2018). Distinct activity-gated pathways mediate attraction and aversion to CO_2 in Drosophila. *Nature*, *564*(7736), 420–424. https://doi.org/10.1038/s41586-018-0732-8

Vilinsky, I., Hibbard, K. L., Johnson, B. R., & Deitcher, D. L. (2018). Probing Synaptic Transmission and Behavior in *Drosophila* with Optogenetics: A Laboratory Exercise. *Journal of undergraduate neuroscience education : JUNE : a publication of FUN, Faculty for Undergraduate Neuroscience*, *16*(3), A289–A295.

Vosshall, L. B., & Stocker, R. F. (2007). Molecular architecture of smell and taste in Drosophila. *Annual review of neuroscience*, *30*, 505–533. https://doi.org/10.1146/annurev.neuro.30.051606.094306

Wagh, D. A., Rasse, T. M., Asan, E., Hofbauer, A., Schwenkert, I., Dürrbeck, H., Buchner, S., Dabauvalle, M. C., Schmidt, M., Qin, G., Wichmann, C., Kittel, R., Sigrist, S. J., & Buchner, E. (2006). Bruchpilot, a protein with homology to ELKS/CAST, is required for structural integrity and function of synaptic active zones in Drosophila. *Neuron*, *49*(6), 833–844. https://doi.org/10.1016/j.neuron.2006.02.008

Wilson, R. I. (2013). Early olfactory processing in Drosophila: Mechanisms and principles. *Annual Review of Neuroscience*, 36, 217–241. https://doi.org/10.1146/annurev-neuro-062111-150533

Winding, M., Pedigo, B. D., Barnes, C. L., Patsolic, H. G., Park, Y., Kazimiers, T., Fushiki, A., Andrade, I. V., Khandelwal, A., Valdes-Aleman, J., Li, F., Randel, N., Barsotti, E., Correia, A., Fetter, R. D., Hartenstein, V., Priebe, C. E., Vogelstein, J. T., Cardona, A., & Zlatic, M. (2023). The connectome of an insect brain. *Science (New York, N.Y.)*, *379*(6636), eadd9330. https://doi.org/10.1126/science.add9330

Wu, Y., Helt, J. C., Wexler, E., Petrova, I. M., Noordermeer, J. N., Fradkin, L. G., & Hing, H. (2014). Wnt5 and drl/ryk gradients pattern the Drosophila olfactory dendritic map. *The Journal of neuroscience : the official journal of the Society for Neuroscience*, *34*(45), 14961–14972. https://doi.org/10.1523/JNEUROSCI.2676-14.2014

Zheng, Z., Lauritzen, J. S., Perlman, E., Robinson, C. G., Nichols, M., Milkie, D., Torrens, O., Price, J., Fisher, C. B., Sharifi, N., Calle-Schuler, S. A., Kmecova, L., Ali, I. J., Karsh, B., Trautman, E. T., Bogovic, J. A., Hanslovsky, P., Jefferis, G. S. X. E., Kazhdan, M., Khairy, K., … Bock, D. D. (2018). A Complete Electron Microscopy Volume of the Brain of Adult Drosophila melanogaster. *Cell*, *174*(3), 730–743.e22. https://doi.org/10.1016/j.cell.2018.06.019

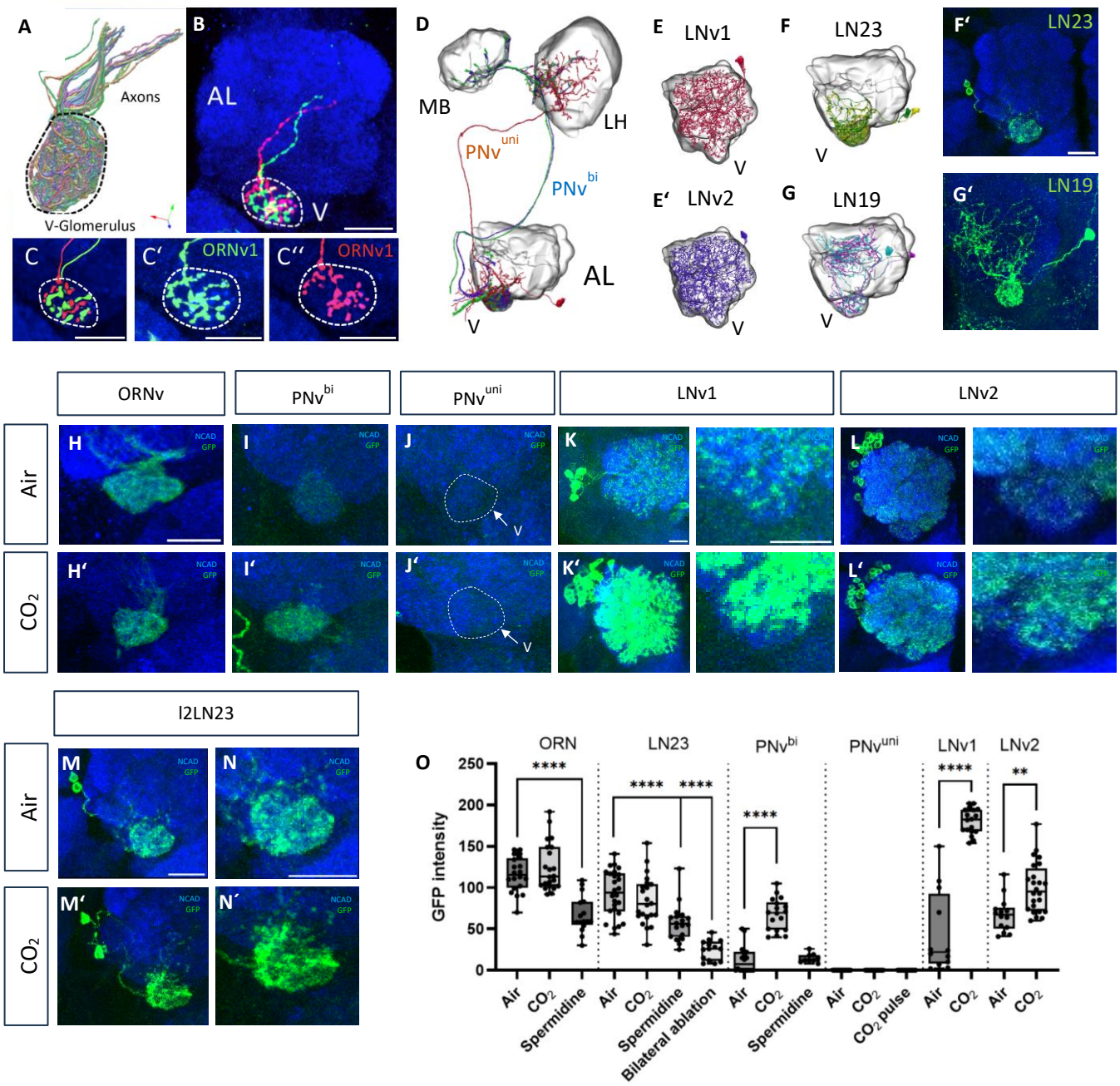

Figure 1. Principal neurons of the V glomerulus show distinct response properties for CO_2. (A–C) About 40 olfactory sensory neurons (ORNv) innervate the ipsilateral V glomerulus at the ventral AL surface (A). Single cell clones revealed the terminal branch pattern of ORNv axons (B). Each ORNv axon forms 3–5 non-overlapping terminal branches (C). **(D–G)** Morphology of central neurons of the V glomerulus, including 2 types of projection neurons (PNv^{uni} and PNv^{bi}, D), 2 classes of broad local interneurons (LNv1 and LNv2, E/E') and 2 classes of sparse LNs (LN23 and LN19, F, G). Gal4 expression lines for sparse interneurons LN23 and LN19 (F', G'). **(H–N)** CaLexA reporter expression in different neuron classes under ambient air (H–N) and elevated CO_2 levels (H'–N'). CaLexA activity could be observed in ORNv, LNv1/2 and LN19, but not in glomerular PNs under ambient air conditions. **(H'-N')** Following chronic CO_2 stimulation, ORNv and LN23 show high activity, comparable to the GFP expression levels at ambient air. Based on the CaLexA-GFP intensity, previous activity was higher for PNv^{bi} following stimulation as was the case for LNv1 and LNv2. PNv^{uni} showed no activity as indicated by the GFP levels. **(O)** Quantification of GFP signal intensity in ORNv, LN23, PNv^{bi}, PNv^{uni}, LNv1, and LNv2. The experimental conditions were, that the flies were either kept in ambient air or in 5% CO_2 for 3 consecutive days. For ORNs, LN23 and PNv^{bi} we also exposed the flies to spermidine, which is a strong GR21a (ORNv) inhibitor. The effect was so strong for LN23, so that we also wanted to compare it to a complete bilateral ablation of both antennae. Further, since continuous exposure to CO_2 did not produce any GFP signal for PNv^{uni}, we tried a pulsed presentation of the CO_2 stimulus, but that also showed no effect. The white bars at the lower right corners indicate the scale of 20 ym. This also applies to the following figures.

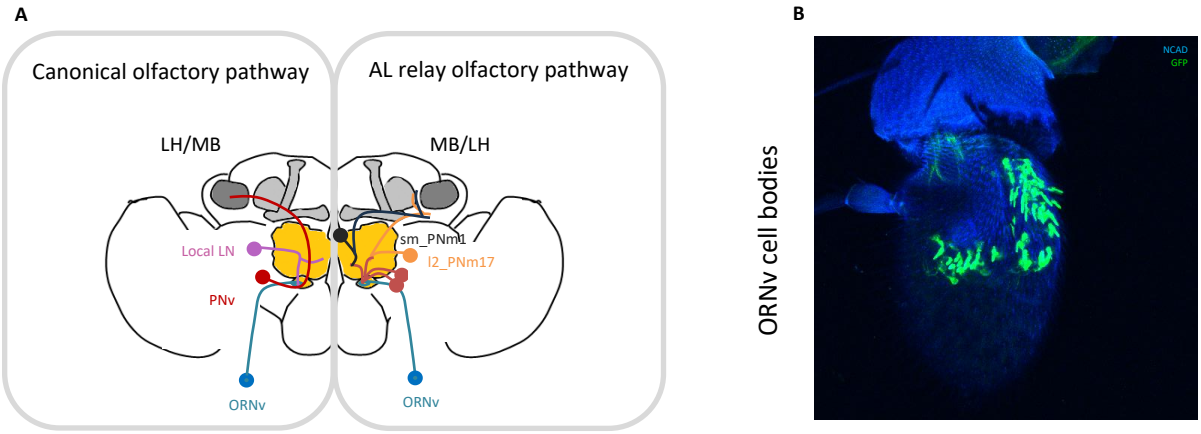

Supplementary Figure 1. (A) Schematic of the canonical olfactory pathway (left) and the identified AL relay pathway (right). **(B)** CaLexA::GFP expression in vORN cell bodies on the 3rd antennal segment.

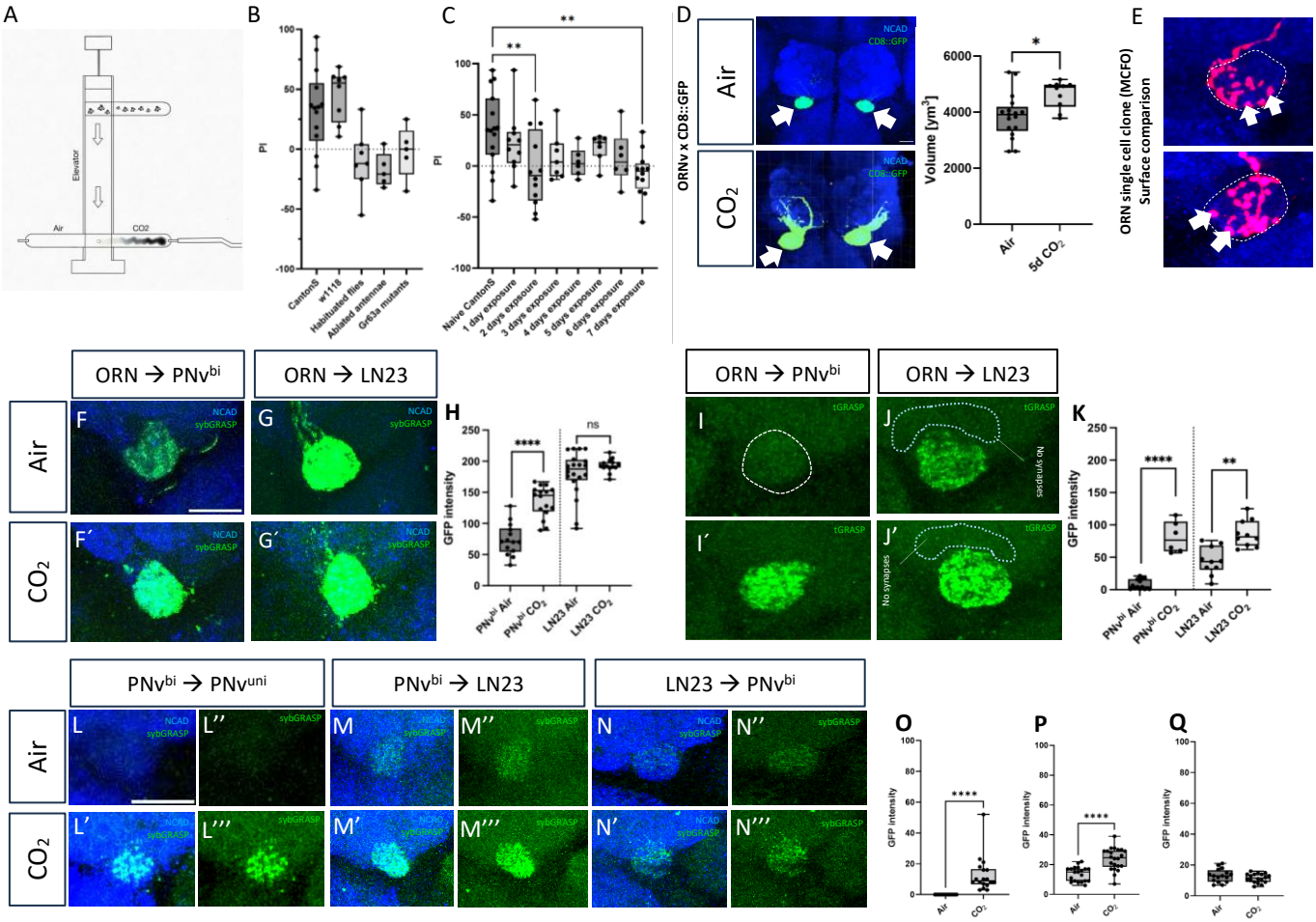

Figure 2. Circuit dynamics of the V glomerulus during CO_2-induced habituation. (A) T-maze setup to determine CO_2 valence identity of adult flies. **(B)** Performance index (PI) of naïve flies compared to flies, which have experienced either chronic CO_2 exposure, removal of both antennae or a mutation of the CO_2 receptor GR63a, each of it leading to a loss of innate aversion response towards CO_2. A value of 100 for the PI represents a 100% attraction towards ambient air for a tested group of flies, while a negative value of -100 would indicate a 100% attraction towards 5% CO_2. **(C)** Temporal pattern of CO_2-induced behavioral habituation. It became evident, that even after 1 day of exposure, that aversion towards 5% CO_2 already decreased drastically. **(D, E)** Structural changes of the V glomerulus volume (D) and axonal arborization of ORNv (E) following 5 days of chronic CO_2 stimulation. **(F–Q)** Synaptic connectivity among neurons of the V glomerulus analyzed by transgenic GRASP. Activity-dependent sybGRASP indicates enhanced ORNv→PNv^{bi} connectivity (F', H), but no significant changes for ORNv→LN23 (G', H) during behavioral habituation. Activity-independent tGRASP expression demonstrates increased synaptic connectivity of ORNv axons with PNv^{bi} and LN23, consistent with morphological changes observed in ORN terminals during habituation (I', J', K). ORN input is restricted to the glomerulus but not seen in the extraglomerular region (arrows, J).Differences in SybGRASP levels among central neurons of the V glomerulus PNv^{bi} neurons showed higher GFP intensity after prolonged exposure to elevated CO_2 levels (O, P compared to Q). The GFP levels for LN23 remained similar to the ambient air control (L-Q)

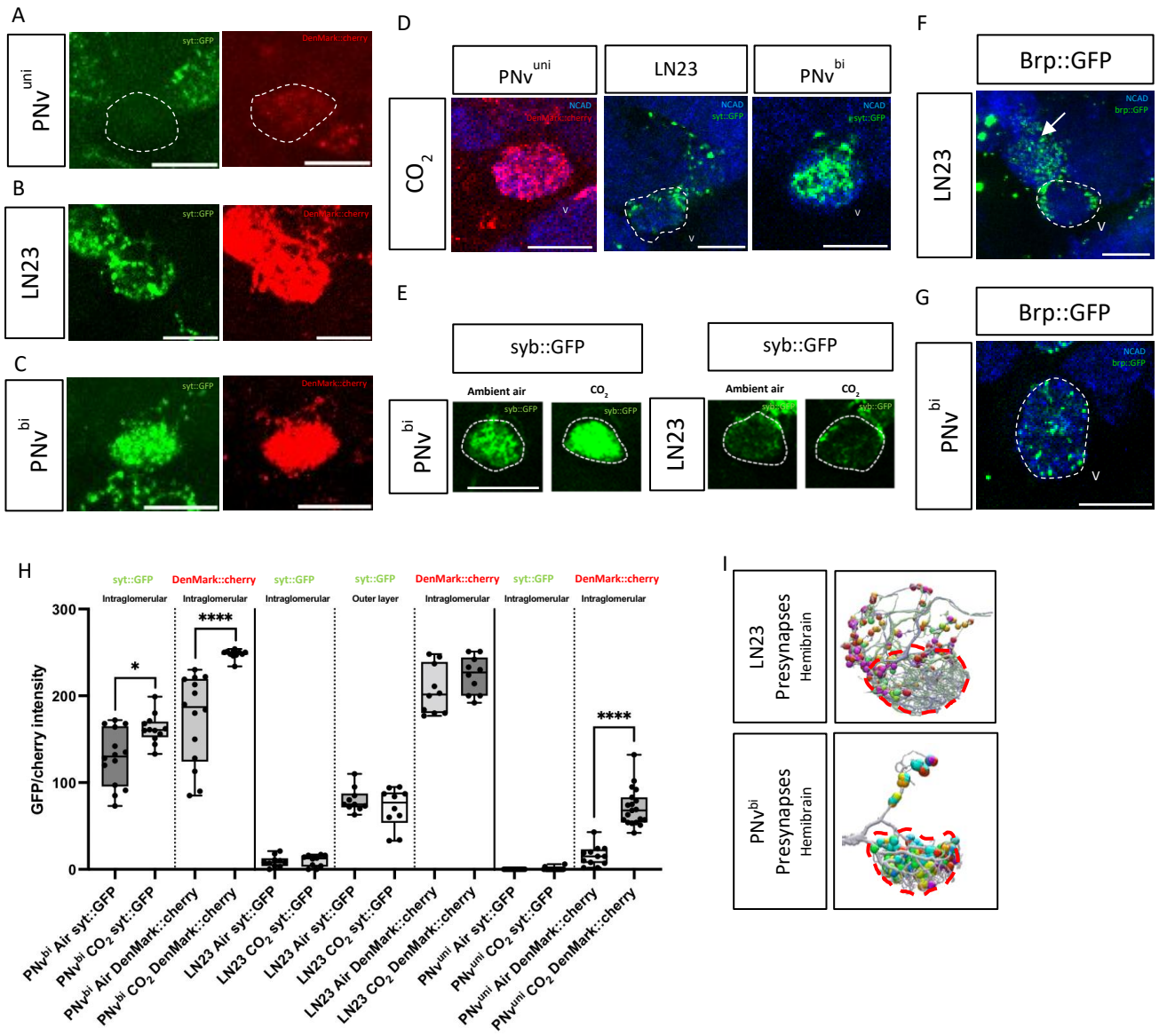

Figure 3. Neuronal polarity of CO_2 glomerular circuit components. (A-C) confocal sections illustrate *syt::GFP* and *DenMark::Cherry* expression in LN23 Quantification of GFP/cherry levels *syt::GFP* and *DenMark::Cherry* revealed distinct localization of presynaptic sites in PNv^{bi}, PNv^{uni}, and LN23. PNv^{bi} displayed prominent presynaptic labeling throughout the glomerular neuropil, while PNv^{uni} showed no detectable presynaptic signal, despite clear dendritic arborizations. LN23 exhibited scattered presynaptic puncta largely outside the glomerular boundaries. **(D)** PNv^{uni} LN23 and PNv^{bi} show different responses following habituation. While LN23 did not show increased *syt::GFP* or *DenMark::cherry* signal, both were increased for PNv^{bi} while for PNv^{uni} only *DenMark::cherry* was amplified . **(E)** *Syb::GFP* labeling further confirmed that presynaptic sites in PNv^{bi} were restricted to the glomerular neuropil and increased after chronic CO_2 exposure, whereas LN23 signals remained scattered along the glomerular margin. **(F-G)** Higher-resolution optical sections confirm the presence of *brp::GFP* puncta in LN23 dendrites outside the V glomerulus **(F, arrow)** but confined to the V glomerulus in PNv^{bi}. **(H)** Quantification of *syt::GFP* and *DenMark::cherry*. For LN23 we differentiated between intensity measurements in the center of the glomerulus and measurements near the glomerular boundary. **(I)** Hemibrain reconstructions show the enrichment of LN23 presynaptic sites (colored spheres) in extraglomerular domains compared to the intraglomerular distribution in PNv^{bi}

A

LN23::GFP

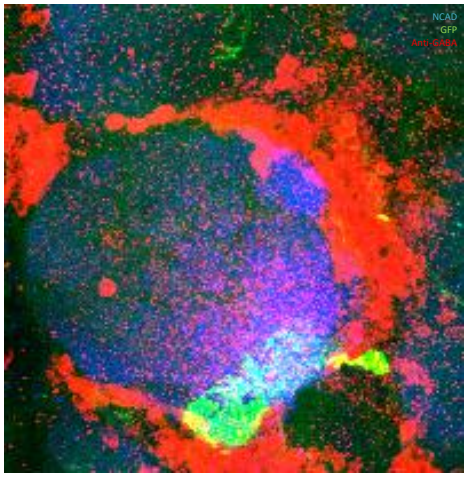

Supplementary Figure 3. (A) CaLexA labeling of LN23 combined with anti-GABA staining revealed no colocalization, indicating that LN23 is not GABAergic.

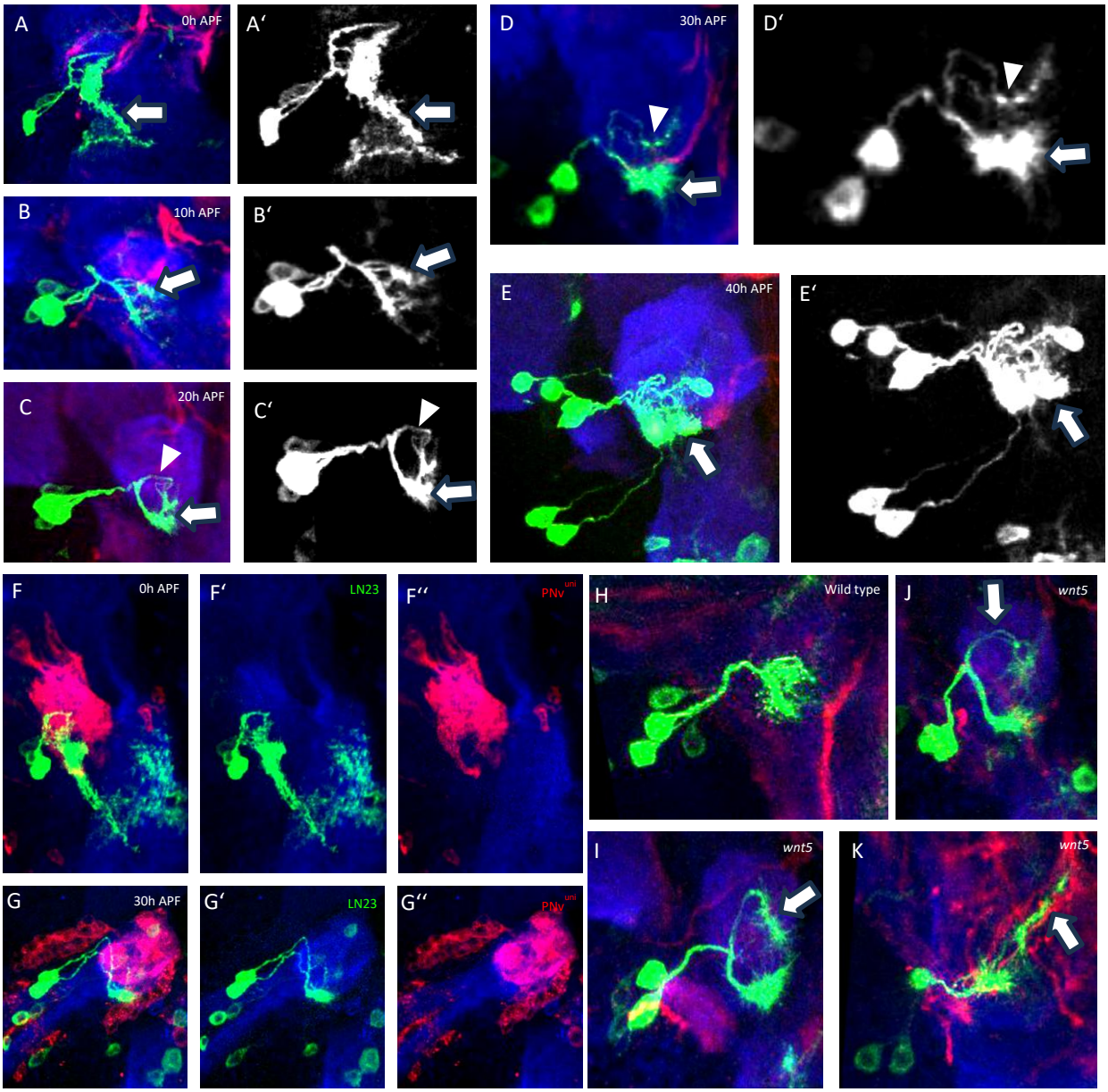

Figure 4. Early LN23 development. (A-E') At the beginning of pupal development (0h APF), larval LN23 neurons remodel their ventral processes (arrow in A) and start extending into the developing adult AL (arrow in B). While a broad arborization can be observed in the ventral AL (arrows in C and D), a small process extends in the dorsal AL to target posterior to the V glomerulus (arrowheads in C and D). At 40h APF, the main LN23 dendrites are restricted to the glomerular boundaries (arrow in E). **(F-G'')** In the reorganization from the larval to adult AL, LN23 processes (green) synchronize with uni-glomerular PN dendrites (red). Compared to wild-type **(H)**, loss of *Wnt5* **(I-K)** leads to a larger separation of ventral and dorsal LN23 branches (arrows in I and J), which later extend along axons towards higher brain centers (arrow in K).

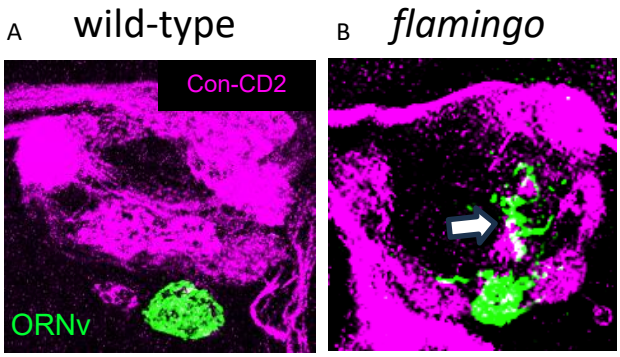

Supplementary Figure 4. Loss of the cell adhesion molecule Flamingo in ORNv. In contrast to the (A) wild-type axonal convergence of ORNv within the glomerular boundaries, (B) *fmi*-mutant ORNv axons overshoot the ventral glomerular domain and extend into the posterior AL (arrow).

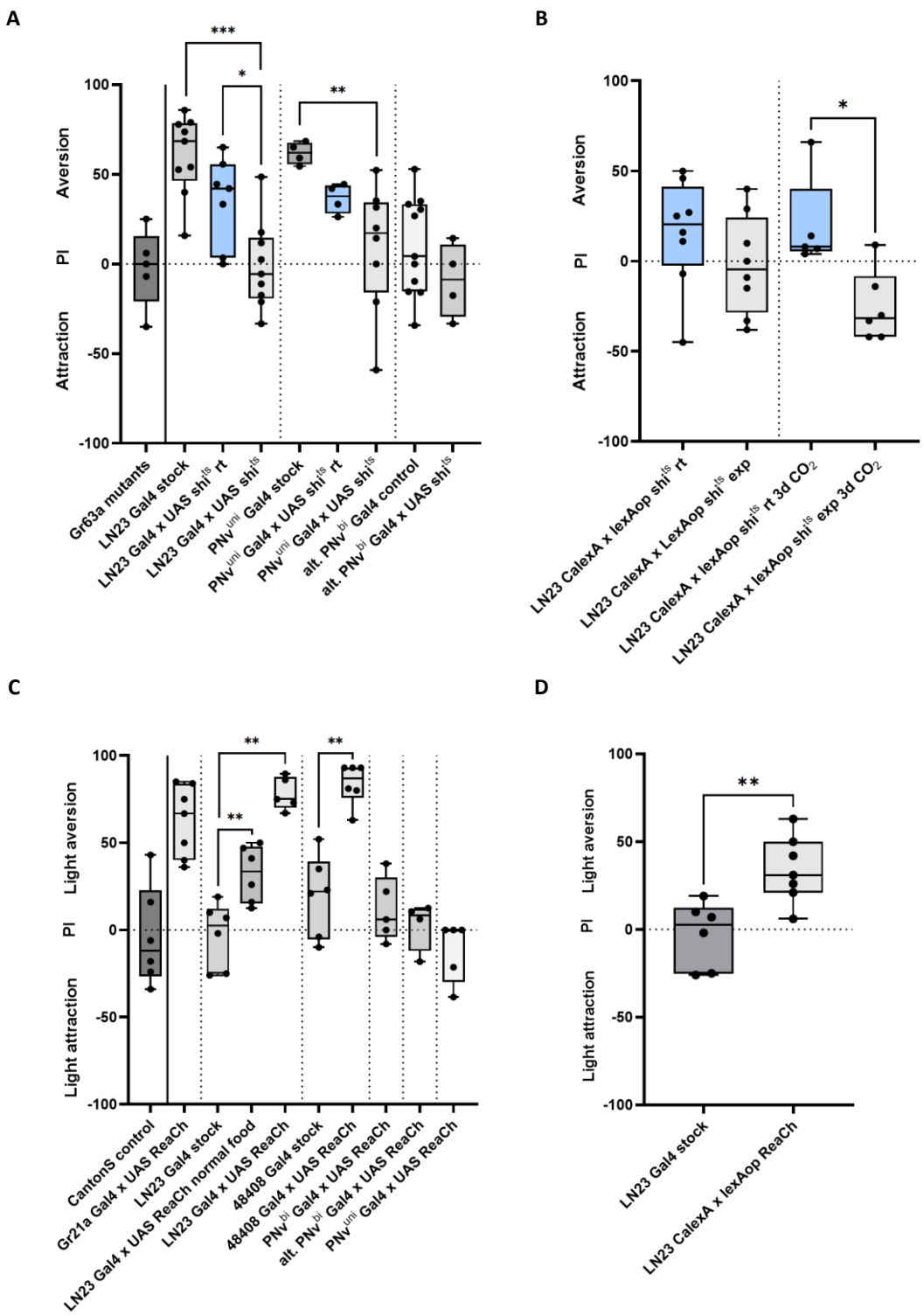

Figure 5. Activity of LN23 controls CO_2 aversion behavior. (A) Cell type–specific silencing with UAS-*shibire*^{ts} revealed that neuronal activity of all three V-glomerulus relay neurons contributes to innate CO_2 avoidance. Silencing of PNv^{uni} or PNv^{bi} reduced avoidance behavior, with a stronger effect in PNv^{uni}. In contrast, LN23 silencing abolished CO_2 aversion entirely. Control experiments performed at room temperature (rt; exp stands for experimental condition at restrictive temperatures), where *shibire*^{ts} should remain permissive, showed partial reduction of avoidance in PNv^{uni} and LN23. Since experiments with PNv^{bi} Gal4 (VT031497) showed inconclusive results, we used the alternative PNv^{bi} (alt. PNv^{bi}) Gal4 driver line (R53A05; BDSC#38859). **(B)** Cell type–specific expression of *shibire*^{ts} via CaLexA confirmed the essential role of LN23 in CO_2 behavior. LN23 CaLexA-*shibire*^{ts} flies showed reduced avoidance, and chronic CO_2 exposure, which should boost CaLexA activity, shifted behavior from avoidance to attraction. **(C)** Optogenetic activation using UAS-ReaChR demonstrated sufficiency of LN23 for driving aversive behavior. Light activation of ORNv (GR21a-Gal4) and LN23 (independent drivers LN23-Gal4 and alternative line 48408-Gal4) triggered robust avoidance, while activation of PNv^{bi} or PNv^{uni} failed to elicit significant changes. **(D)** CaLexA-driven ReaChR expression in LN23 also induced light-mediated aversion, confirming cell type specificity.

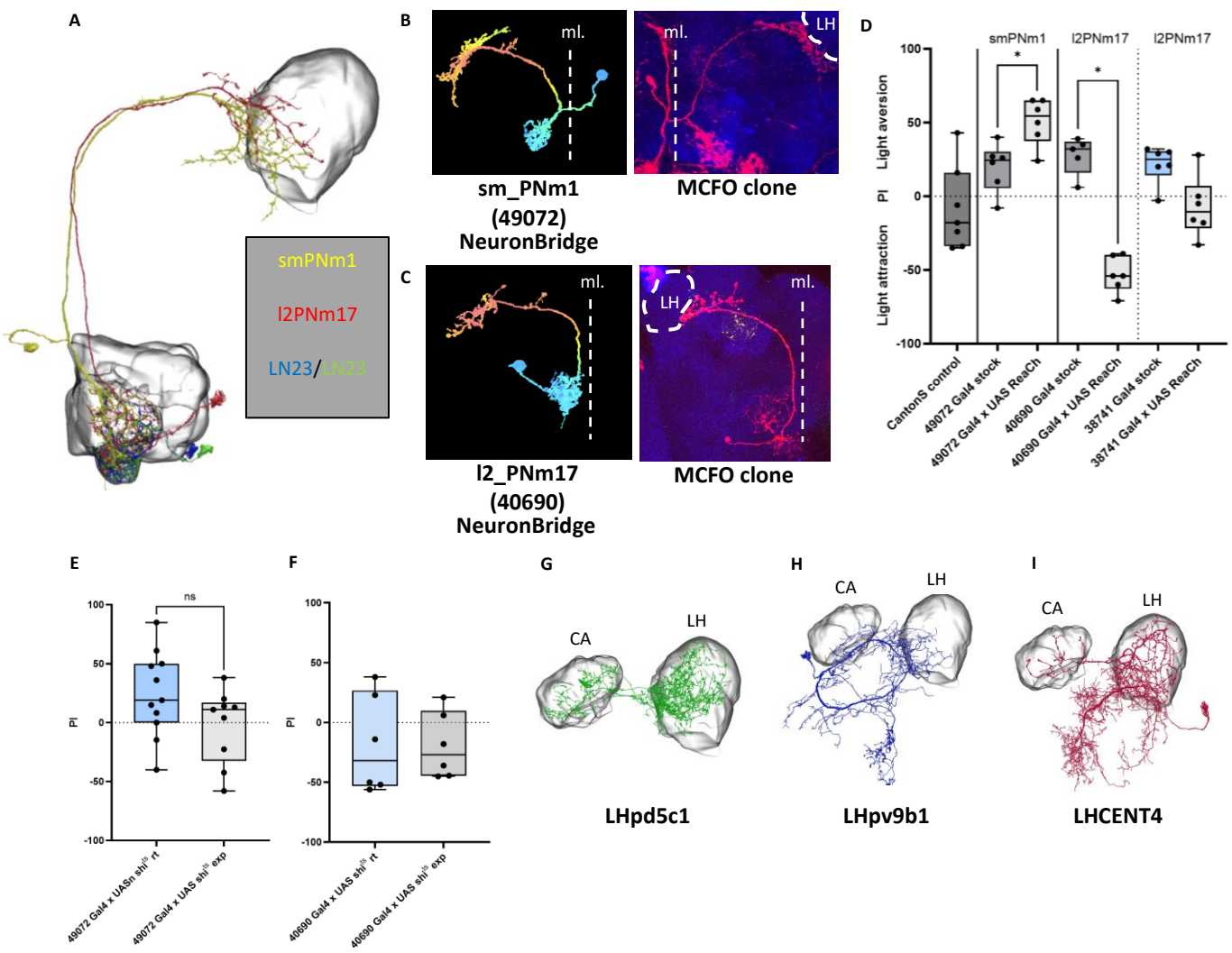

Figure 6. Two postsynaptic neurons of LN23 convey opposing odor valence. (A) Connectomic analysis (neuPrint, Janelia Research Campus) revealed two major postsynaptic partners of LN23, PNm1 and PNm17. **(B, C)** Single-cell MCFO clones of sm_PNm1 and l2_PNm17 show axonal projections bypassing the canonical olfactory lateral horn (LH) and targeting adjacent regions including the posterior lateral protocerebrum (PLP), superior clamp (SCL), and superior lateral protocerebrum (SLP). **(D)** Optogenetic activation of PNm1 induced strong aversion, whereas PNm17 activation elicited attraction, demonstrating opposing behavioral valence. **(E, F)** Silencing experiments with *shibire*^{ts} confirmed that CO_2 aversion requires PNm1 activity but is unaffected by PNm17 silencing. **(G–I)** Hemibrain connectome data identified distinct downstream LH partners for the two CO_2 relay pathways: LHPD5c1 as the primary postsynaptic target of PNv^{bi}, LHPV9b1 downstream of PNm1, and LHCENT4 downstream of PNv^{uni}. The abbreviation "rt" stands for the room temperature control of *shibire*^{ts} while "exp" is the experimental condition at the restrictive temperature. The midline in the brain is indicated by the dashed line and "ml.".

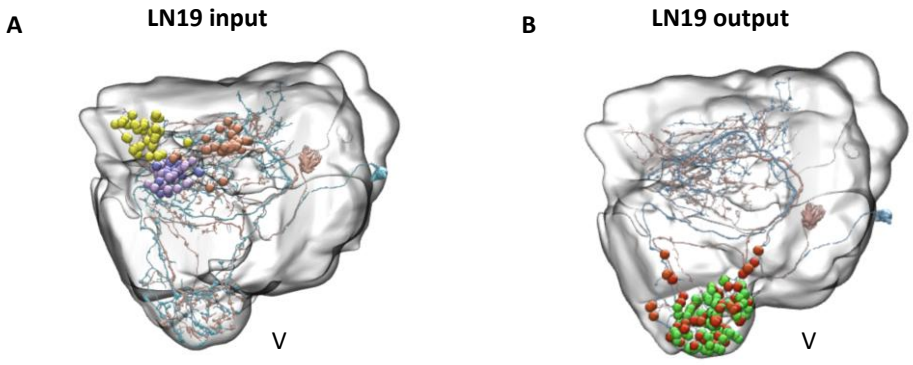

C

Postsynaptic partner	# of connections		Presynaptic partners	# of connections
PNv^{bi}	223		ORNv	292
ORNv	201		ORN_VM7v	128
vLN24	158		VM7d_adPN	91
VM7d_adPN	140		ORN_DC4	72
PNv^{uni}	134		DM4_adPN	43

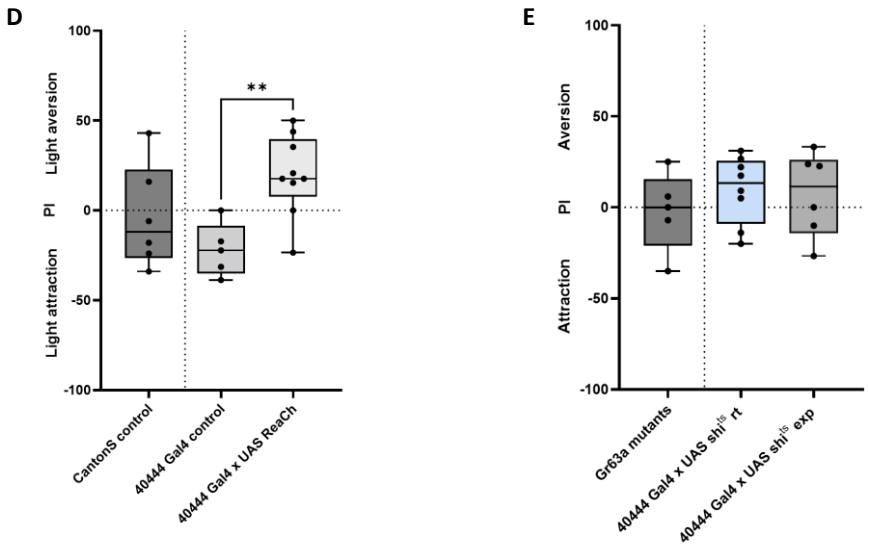

Figure 7. The "food" odor associated l2LN19. (A) LN19 gets input from DM4, DC4/DP1 and VM7 while **(B)** the output is within the V glomerulus. **(C)** Table illustrating the post,- and presynaptic partners of LN19 as they can be found on https://neuprint.janelia.org/ **(D)** Optogenetic activation of LN19 using a specific driver line induced strong behavioral aversion, indicating that LN19 activity can bias olfactory responses towards avoidance. **(E)** In contrast, silencing LN19 via shibire^{ts} did not alter innate CO_2 avoidance, suggesting that while LN19 is sufficient to promote aversive responses, it is not essential for baseline CO_2-driven behavior. The abbreviation "rt" stands for the room temperature control of shibire^{ts} while "exp" is the experimental condition at the restrictive temperature.

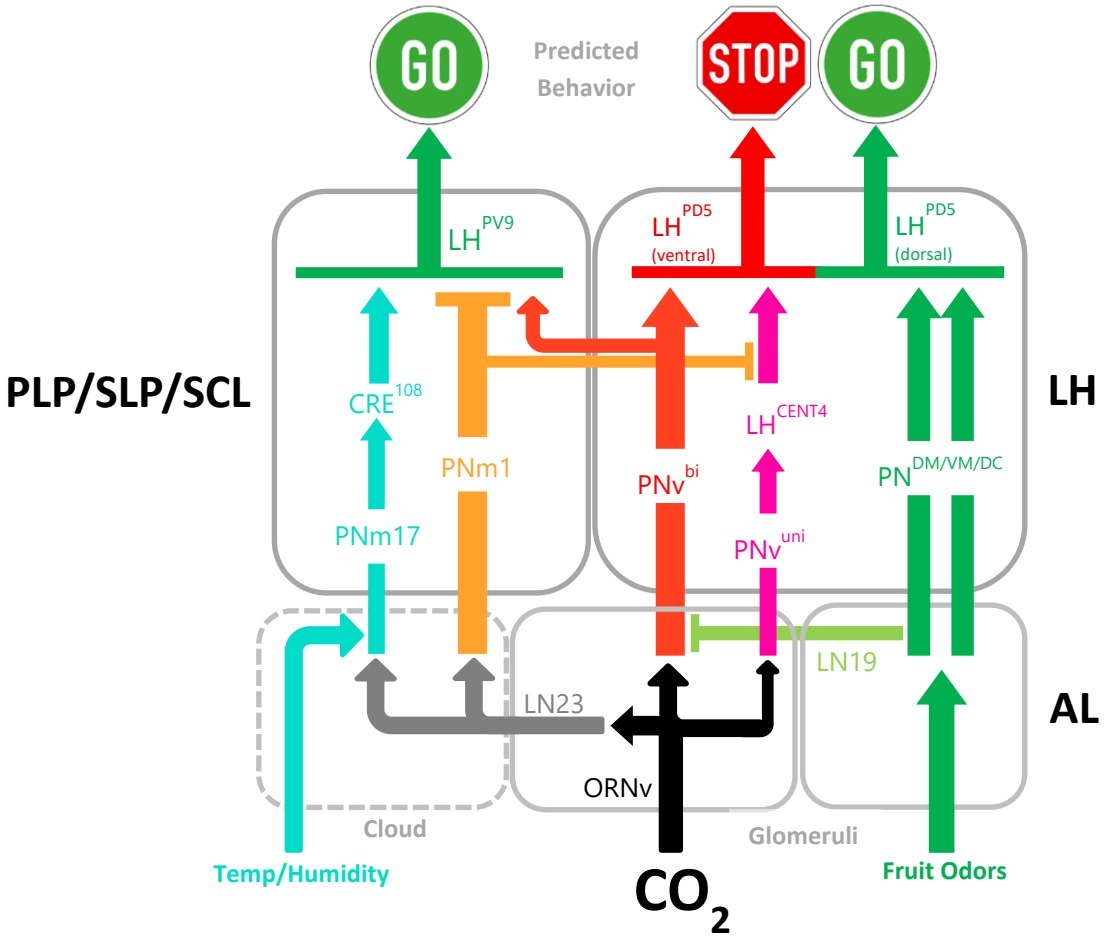

Figure 8. Convergence of parallel channels for CO_2 valence coding. The activity of CO_2-responsive sensory neurons (ORNv, black) is relayed by 4 parallel PN channels to converge onto 2 central brain target neurons of opposite intrinsic valence identity. First, the glomerular PNv^{bi} (red) and PNv^{uni} (pink) target the ventral domain of LH^{PD5} (directly or via LN^{cent4}, respectively) to trigger behavioral aversion (red). Second, the extraglomerular PNm1 (yellow) and PNm17 (turquoise), activated via the lateral LN23 relay (gray), converge onto LH^{PV9} (directly or via CRE^{108}, respectively) which mediates attraction (green). While PNm17 supports LH^{PV9} activity, GABAergic PNm1 blocks LH^{PV9} thereby resulting in an aversive response. This core aversion domain (PNv^{bi}/PNv^{uni}/PNm1) can be modified either via the activation of the dorsal LH^{PD5} domain by fruit odor PNs ($PN^{DM/VM/DC}$, green) or an increase of PNm17 by non-olfactory sensory neurons (turquoise). PNv^{bi} is providing balancing activity between channels, for example through direct input onto LH^{PV9} or via receiving LN19-mediated inhibition by food PNs.